Fluid–Structure Interaction of a thin cylindrical shell filled with a non-Newtonian fluid

Antonio Zippo, Giovanni Iarriccio, Luca Bergamini, Elena Colombini, Paolo Veronesi, Francesco Pellicano

Fluid-Structure Interaction of a thin cylindrical shell filled with a non-Newtonian fluid

Authors:

Zippo Antonio

University of Modena and Reggio Emilia, 41121 Modena, Italy.

InterMech MoRe Centre, 41121 Modena, Italy.

ORCID id: 0000-0001-6206-2619

Iarriccio Giovanni

University of Modena and Reggio Emilia, 41121 Modena, Italy.

InterMech MoRe Centre, 41121 Modena, Italy.

ORCID id: 0000-0001-9323-8656

Luca Bergamini

University of Modena and Reggio Emilia, 41121 Modena, Italy.

InterMech MoRe Centre, 41121 Modena, Italy.

ORCID id: 0000-0001-7786-1499

Elena Colombini

University of Modena and Reggio Emilia, 41121 Modena, Italy

ORCID id: 0000-0002-0268-8027

Paolo Veronesi

University of Modena and Reggio Emilia, 41121 Modena, Italy.

ORCID id: 0000-0003-3095-6495

Pellicano Francesco

University of Modena and Reggio Emilia, 41121 Modena, Italy.

InterMech MoRe Centre, 41121 Modena, Italy.

ORCID id: 0000-0003-2465-6584

Corresponding Author

Zippo Antonio, antonio.zippo@unimore.it

N. of pages: 46

N. of figures: 25

N. of tables: 2

Abstract

This paper presents the results of an extensive experimental campaign on the dynamic interactions between an elastic structure and a non-Newtonian fluid. The structure consists of a thin circular cylindrical shell, with the bottom end clamped to a shaking table, and the top end carrying a heavy mass. The fluid is a mixture of water and cornstarch, also known as oobleck. The system dynamics has been analysed in the presence of different fluid levels (i.e., empty, partially, and full-filled). The experimental modal analysis has been carried out to identify the modal properties of the system. High energy tests have been performed by means of a seismic excitation consisting in a stepped sine sweep, spanning the forcing frequency within the neighbourhoods where strong resonance phenomena take place. Different excitation amplitudes have been considered in order to induce phase transitions in the fluid, and the onset of complex dynamics has been detected using Fourier spectra and bifurcation diagrams of the Poincaré maps: when the fluid-solid transition occurs, the entangled non-Newtonian fluid rheology results in a complex dynamic scenario where period-doubling cascades, quasiperiodic and chaotic responses can be observed.

Keywords

Fluid-structure interaction; non-Newtonian fluids, nonlinear vibrations, shells, complex dynamics, experiments.

1. Introduction

Fluid-structure interaction (FSI) phenomena are of interest in several fields, from Mechanical Engineering to Medical Science. The FSI can cause dramatic changes in the dynamic response of a system and static and dynamic instabilities can arise, such as the flutter of airplane wings or the interaction between the human aorta and the blood.

The literature on the FSI is mainly focused on the interactions between elastic structures and Newtonian fluids. Nevertheless, there are many examples where the Newtonian fluid models cannot be considered, as in the case of blood or toothpaste.

The present work involves three topics: i) shell dynamics, ii) fluid-structure interaction, and iii) non-Newtonian (NN) fluids.

In the following, a literature review is given to provide a solid background.

In 1983, Babcock [1] published a review paper counting about 50,000 papers on shell stability claiming that the open topics were: experimental investigations, sensitivity to imperfections, plastic and dynamic buckling, and post-buckling. Despite this large number of papers, Refs. [2-6] pointed out the need for further research on the dynamics and stability of shells, which were not well understood topics.

For a deep analysis of models and phenomena associated with shell vibrations, covering a wide range of cases in the linear and nonlinear fields, see Refs. [7, 8].

Theoretical works using Donnell's nonlinear shallow shell theory for studying the instabilities due to axial periodic loads and seismic excitations are given in Refs. [9,10].

Nagai and Yamaki [11] studied the parametric oscillations of circular cylindrical shells; they clarified that when the membrane approximation is used in calculating the in-plane stresses, the model leads to excessive errors when axisymmetric modes are resonant.

Bondarenko and Galaka [12] published experimental results on shells instabilities due to parametric excitations, a particularly violent phenomenon was observed when the principal parametric instability region is met, they defined the phenomenon as a "bang" to stress the sudden appearance of a very strong noise; the authors were not able to give a clear explanation of the experimental observations.

Further studies on the parametric excitation of thin circular cylindrical shells can be found in Refs. [13-16], and comparisons among the different shell theories are discussed in Refs. [17, 18].

Recent studies on the dynamic instabilities of cylindrical shells can be found in Refs. [19-24], where the Sanders-Koiter theory has been used for modelling the strain-displacement relationships. A good agreement between theories and experiments was shown, and the role of the axial load on the onset of chaotic vibrations, with an associated extreme noise production, was clarified.

Regarding the FSI in the presence of inviscid and Newtonian fluids, Païdoussis reported and discussed a variety of models and applications in his seminal two-volume treatise [25, 26].

In 2003 Amabili and Païdoussis [27], reviewed more than 300 papers on the nonlinear vibrations of shells with or without FSI, highlighting the lack of experimental results.

In Refs. [28-31], the nonlinear vibrations and stability of a circular cylindrical partially filled tank were investigated through theoretical models. By considering Donnell's shell theory along with the potential theory for an inviscid and incompressible fluid, the internal resonance between sloshing and shell modes was addressed.

Gonçalves and Batista [32] analysed the nonlinear dynamics of fluid filled shells. By using Sanders' nonlinear theory of shells with a multimode expansion and retaining the potential flow assumption, the authors showed how the presence of a dense fluid within the shell leads to an increment of the softening nonlinearity compared to the same shell in vacuo.

Experiments on partially water-filled and partially submerged shells are given in Ref. [33]. The results evidenced both softening and hardening type nonlinearity, depending on the mode shape and the level of water filling.

Chiba [34-36] investigated the large-amplitude vibrations of polymeric vertical circular cylindrical shells partially filled with water to different levels. It was observed that the strongest nonlinearity happens for the fundamental mode. Similarly, higher nonlinearity is observed for shorter circular cylindrical shells. Intermediate liquid levels show higher nonlinearity than empty or full filled shells. Traveling waves were observed

experimentally when conjugate (double) modes are excited, both in the case of sloshing and bulging modes. Interesting experimental expedients were described in the paper, for example the use of a thin film on the water surface. Further experimental and numerical results, with discussions on traveling waves and internal resonance, are reported in Refs. [37-39].

A finite element method was proposed in Ref. [40] to study FSI problems and nonlinear dynamics of open cylindrical shells; inviscid and incompressible fluids were considered.

Using a semi analytical model based on the Donnell shallow shell theory for the structure and the potential flow theory for the inviscid and incompressible fluid, Amabili et al. [41-46] published a series of papers where the effect of a quiescent or flowing heavy fluid was investigated. Further investigations focused on the interactions of circular shells with supersonic flows, compressible, annular, and unbounded flows can be found in Refs. [47-50]; in such a series of studies the presence of compressive forces was accounted for as well [51].

Païdoussis [52] presented at the IUTAM Conference an interesting work where some paradoxes in FSI were discussed.

Muha and Canić [53] presented a theoretical study on the existence of the solution to the FSI problem consisting of an incompressible viscous (Newtonian) fluid interacting with an elastic pipe modelled through Koiter's shell model.

Balasubramanian et al. [54] analysed the nonlinear vibrations of a very soft (corrugated) circular cylindrical shell made of polymeric material, filled with pressurized water; the study was experimental, and a phenomenological model was used for the identification of nonlinear stiffness and damping.

Girchenko et al. [55] studied numerically the interaction of a nonlinear pseudoplastic fluid, with a helical shell. They combined the commercial software FlowVision (finite volumes) and Simulia ABAQUS (finite elements) for showing the differences between Newtonian and NN flows in terms of stresses on the helical structure. Another study regarding FSI and NN fluids was focused on arterial bypass [56], where the effects of wall

elasticity and NN fluid rheology were investigated numerically through the commercial software ANSYS.

The experimental study on the rheology and processing of solvent-free core shell “polymer opals”, given in Ref. [57], analysed an elastic shell grafted to hard colloidal polymer core particles in order to study the optical properties under deformation.

Wu et al. [58] presented a numerical study on the interaction between elastic multi-layered spheres and a NN fluid. They analysed gold nanospheres immersed in water and calculated theoretically the natural frequencies and quality factors.

The literature analysis clearly shows that, even though many publications can be found about FSI problems, and many papers are available about NN fluids, the interaction between vibrating structures and NN fluids appears to be an almost unexplored field.

The goal of the present paper is to give a contribution toward filling the knowledge gap. A series of experiments has been carried out on the dynamic interactions between a polymeric circular cylindrical shell and a NN fluid consisting of a mixture of corn starch flour and water (Oobleck), which is a dilatant fluid. Low energy tests have been carried out to identify the system modal properties. Numerous experiments have been conducted to analyse the behaviour of the systems in resonance conditions, when the amplitudes of vibration become high, and the waves induced into the fluid cause state transitions and complex interactions. Finally, the results are reported and discussed through frequency response diagrams, bifurcation diagrams of Poincaré maps, spectra, and phase portraits.

2. Experimental setup and test procedure

The test specimen consists of a thin polymeric circular cylindrical shell filled with a NN fluid. The shell axis is vertical, the shell bottom is clamped to a shaking table, and a rigid disk closes the top of the shell, see Fig. 1(a,b). The specimen dimensions and material properties are listed in Table 1.

(a) (b)

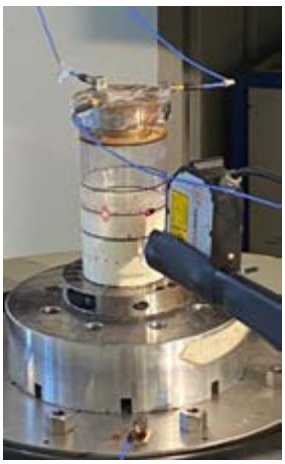

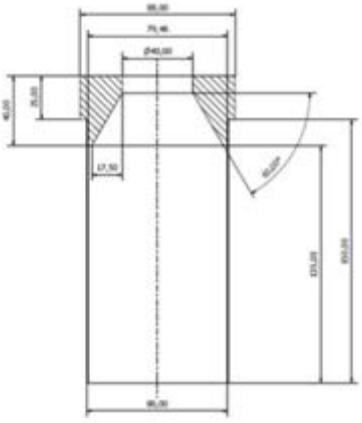

Fig. 1. (a) Test specimen partially filled with oobleck, and (b) shell-disk assembly technical drawing.

Table 1. Specimen geometric dimensions and material properties.

Shell			
	Material		PET
	Density	ρ_S	1366 kg/m^3
	Young modulus	E	3.2·10^9 Pa
	Length	L	0.135 m
	External radius	R_e	0.040 m
	Thickness	h	0.38·10^{-3} m
Top disk			
	Material		Steel
	Mass	m_D	1.34 kg

In Fig. 2, a scheme of the test setup is shown. An electrodynamic shaker, controlled in an open-loop configuration, has been used for imposing a seismic excitation to the test specimen, and the measurement of the actual base excitation has been guaranteed by an accelerometer fixed to the shaker base. Three accelerometers have been placed

on the top surface of the top-mass, close to its circular edge and angularly spaced by 120°. The purpose of these sensors is to measure the acceleration of the disk in the vertical direction (along the shell axis) since, under resonance conditions, this acceleration can be different with respect to the base vibration. In addition, from the correlation of the signals measured by these accelerometers, one could detect possible rotations of the top disk about the shell axis and beam modes.

The vibrometer and telemeter have been used for measuring the shell vibrations in the radial direction, i.e., orthogonal to the shell surface. The laser beam of both sensors focuses on points at half-length of the shell and, to avoid redundancies in the measurements of the velocity (vibrometer) and displacement (telemeter) of the shell wall for a wide range of possible radial modes that can be excited in the non-linear regime, an angle of 57° between the vibrometer and the telemeter has been chosen.

To identify natural frequencies, mode shapes, and the frequency bands where the most important dynamic phenomena due to linear and nonlinear resonances could take place, the modal analysis has been performed through the roving hammer method (i.e., low energy and broadband excitations) and prior to the harmonic base excitation test.

The second part of this study has been dedicated to the nonlinear dynamic scenario. A stepped sine motion has been imposed to the shaker base and high-energy tests have been carried out. The excitation frequency has been varied in the neighbourhoods of the resonance frequency of the first axisymmetric mode, as identified from the modal analysis. The shell has been tested under different conditions of shaker input voltage (i.e., different base acceleration amplitudes), and the forcing frequency has been swept in the range 150-270Hz in both upward and downward directions with a step of 1 Hz. The sampling frequency has been set to 12800 Hz to guarantee enough samples-per-forcing period. Thus, the minimum value of the samples-per-forcing period is 47 at the maximum excitation frequency (270 Hz).

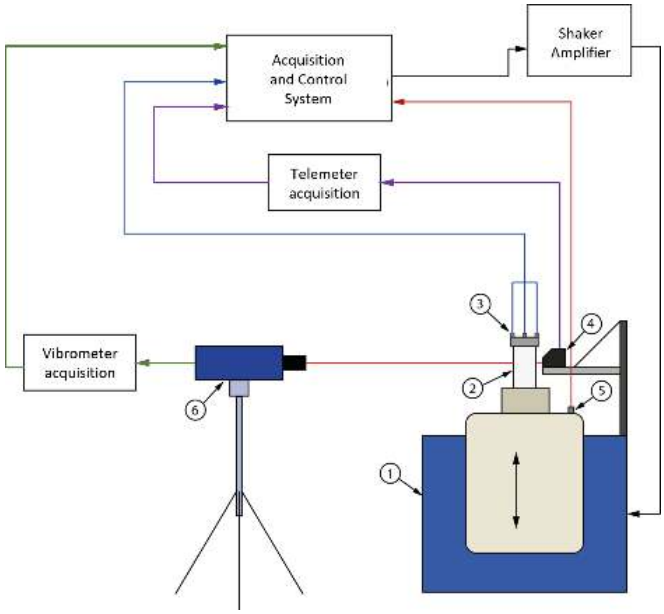

Fig. 2. Test setup scheme: (1) electrodynamic shaker, (2) specimen, (3) top disk accelerometers, (4) laser telemeter, (5) base accelerometer, (6) laser vibrometer.

3. Results

3.1. Low energy test: modal analysis

In this subsection, the modal analysis results are given. Following the well-established notation, the shell-like mode shapes are identified by the number of longitudinal half-waves (*m*), and the number of nodal diameters (*n*). Because of the symmetry, shell structures exhibit conjugate modes (*c*), i.e., modes with same frequency and number of nodal diameters but angularly shifted of $\pi/2n$. Experimentally, the presence of imperfections in the test specimen leads to the splitting of frequencies between conjugate modes. It is worth noting that a generic axisymmetric mode having no waves in the circumferential direction, i.e., no nodal diameters, is identified by (m, 0).

The modal parameters have been identified through the PolyMax algorithm [59], and Table 2 reports the first eight natural frequencies, mode shapes, and modal damping ratios for the three investigated cases: i) empty shell, ii) half-filled shell with oobleck, and iii) full filled shell with oobleck.

For the empty shell carrying the top mass, a comparison of the experimental results with the numerical ones obtained from a finite-element analysis (FEA) is given. The comparison shows a good matching for the first three modes, while discrepancies can be observed for the shell-like modes (<10%). The first mode of vibration involves the lateral bending of the structure; therefore, this mode shows similarities with the first flexural mode of a cantilever beam, see Fig. 3(a, b). The second mode is axisymmetric with one half-wave in the longitudinal direction, Fig. 3(c, d). The third mode involves mainly a pure rotation (tilting) of the top mass with respect to a transversal axis, Fig. 3(e, f). After the tilt mode, the structure exhibits shell-like modes, Fig. 3(g, h), characterized by the presence of one or more circumferential waves ($n \neq 0$).

Table 2. Numerical (FEM) and experimental mode shapes, natural frequencies (f), and linear damping ratios (ζ).

Test case	Mode shape	FEM	Experimental	
	(m, n)	f [Hz]	f [Hz]	ζ [%]
Empty shell				
	Beam-like	55.06	56.58	0.71
	(1,0)	233.49	235.47	0.85
	Tilt	396.00	394.63	0.87
	(1, 5)	596.09	643.09	0.93
	(1, 5, *c*)	-	652.57	1.10
	(1, 4)	619.16	677.21	1.23
	(1, 6)	716.54	780.15	1.04
	(1, 6, *c*)	-	784.82	1.06
Half-filled shell				
50% empty				
50% oobleck				
	Beam-like	-	55.63	0.52
	(1, 5)	-	182.90	1.30
	(1, 6)	-	222.67	1.65
	(1, 0)	-	232.08	1.03
	(1, 3)	-	236.81	1.59
	(1, 7)	-	283.48	1.76
	(1, 2)	-	331.09	1.57
	Tilt	-	367.14	1.00
Full-filled shell				

100% oobleck

Beam-like	-	53.27	1.05
(1, 4)	-	130.44	2.64
(1, 5)	-	136.49	2.96
(1, 3)	-	165.49	1.97
(1, 6)	-	183.81	2.45
(1, 6, *c*)	-	189.57	2.63
(1, 2)	-	225.90	1.67
(1, 0)	-	238.77	1.47

	FEM	Experimental
	(a)	(b)
Beam	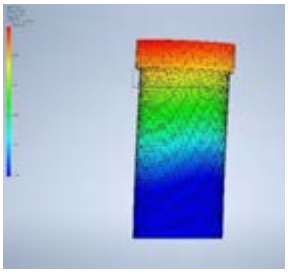	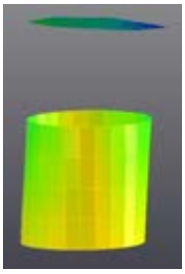
	(c)	(d)
(1,0)	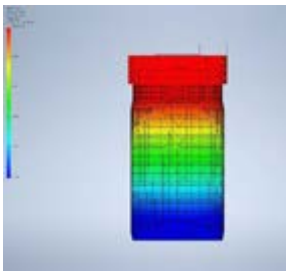	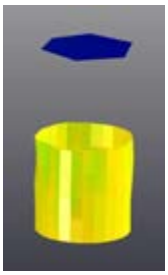

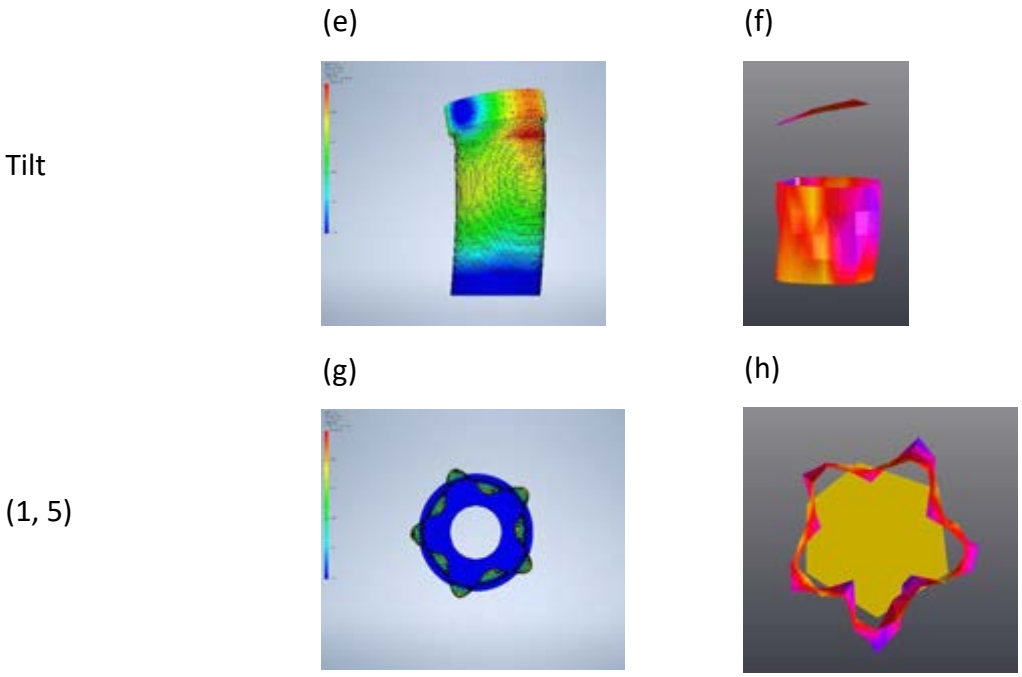

Fig. 3. Empty shell mode shapes: (a, b) cantilever beam-like mode, (c, d) first axisymmetric mode, (e, f) tilt mode, and (g, h) first shell-like mode.

In Fig. 4(a-c), the sum of the FRF amplitudes is displayed for the range 20 Hz-270 Hz. For the empty shell, Fig. 4(a), low frequency modes are the cantilever beam-like mode and the tilt, while no shell-like modes can be observed. When the shell is half-filled with oobleck, the order of the modes is altered, Fig. 4(b). The presence of the fluid leads to an added modal mass effect that causes an abrupt decrease in the natural frequencies of the shell-like modes. Interestingly, one can observe that the natural frequencies of the beam tilt modes are not affected by the presence of the NN fluid. For the full-filled shell, the beam mode is still the first mode of vibration of the system, while a further decrease in the natural frequencies of the shell-like modes takes place and the highest amplification is related to the shell mode (1,6) as visible from Fig. 4(c).

(a) (b)

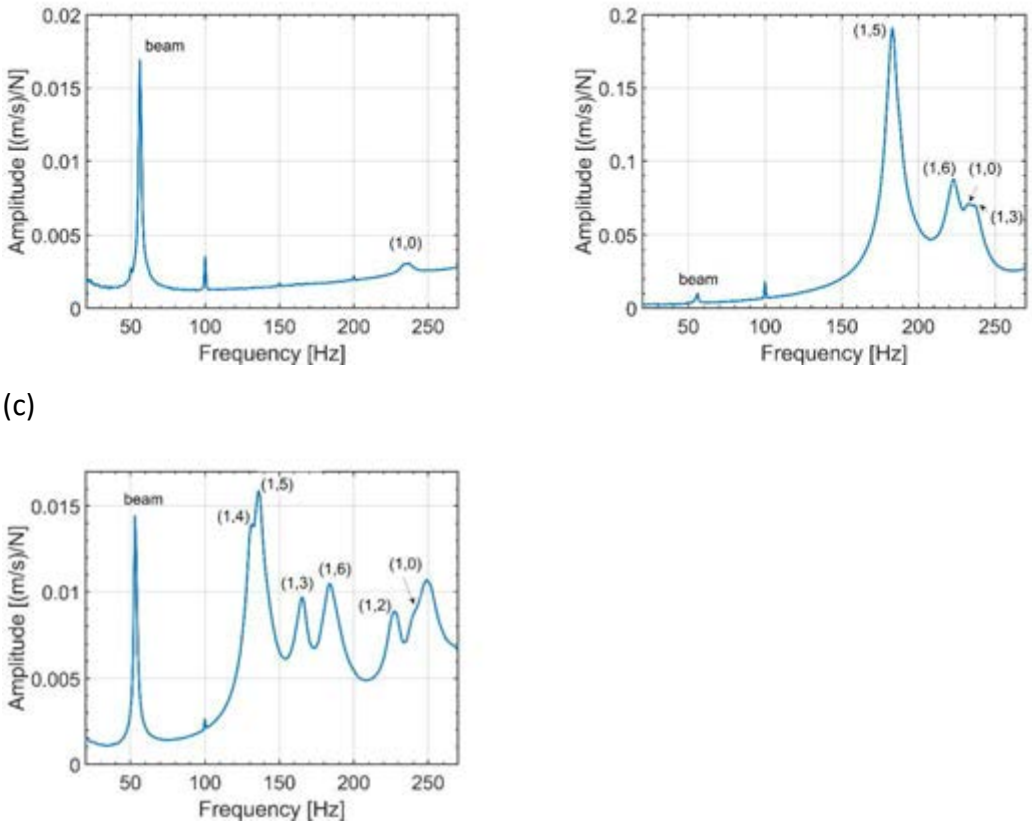

Fig. 4. Sum of the experimental FRFs. (a) empty shell, (b) half-filled and (c) full-filled shell with NN fluid.

3.2. High energy test: harmonic base excitation

3.2.1. Frequency response diagrams: empty shell VS non-Newtonian fluid filled shell

The results obtained by forcing the shell with a base motion are presented herein, and the frequency-response curves of the empty shell are compared to the full-filled shell with oobleck, Fig. 5(a, d). To investigate the role of the NN fluid on the overall system response, the signal provided to the shaker amplifier is harmonic, and different conditions of shaker input voltage amplitudes (0.01 V-0.03V) have been considered. By limiting to the downward frequency variation case, the analysis of the empty shell shows that the resonance of the axisymmetric mode (1,0) at 233.49 Hz gives rise to large amplitude of vibration and a saturation of the top disk vibration at about 600 m/s^2 takes place, Fig. 5(b). According to Refs. [23, 24, 60], this phenomenon leads to an energy transfer from longitudinal to lateral vibration. The analysis of the NN fluid filled shell shows a different scenario. The saturation disappears and, considering a shaker input voltage of 0.03 V, a parametric resonance is visible between 173-205 Hz, Fig. 5(b). This strong resonance results in an amplification of the base acceleration of about ten times in the vertical direction and involves the shell-like modes: the shell lateral response in Fig. 5(c, d), reveals different frequency bands where phenomena related to the fluid phase transitions occur, and the amplitude of vibrations is one order of magnitude higher than the case of empty shell, although the forcing amplitude trend does not change among the different cases as displayed in Fig. 5(a).

(a) (b)

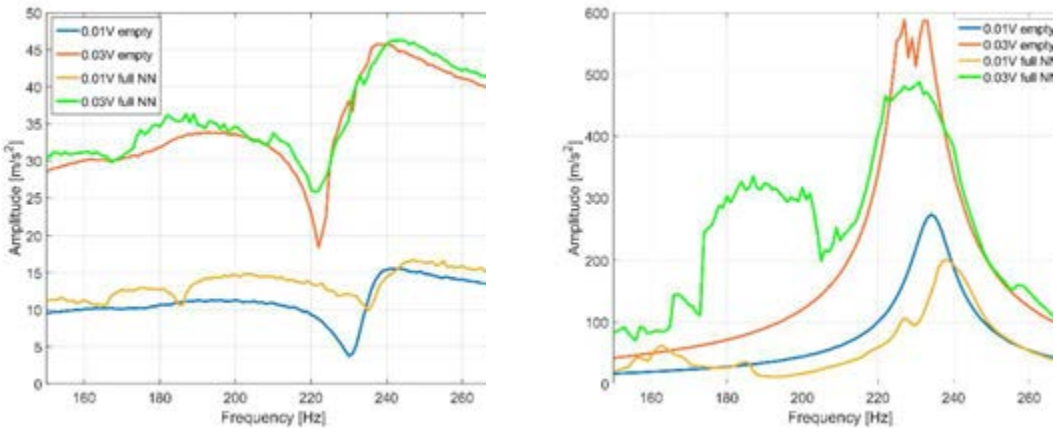

(c) (d)

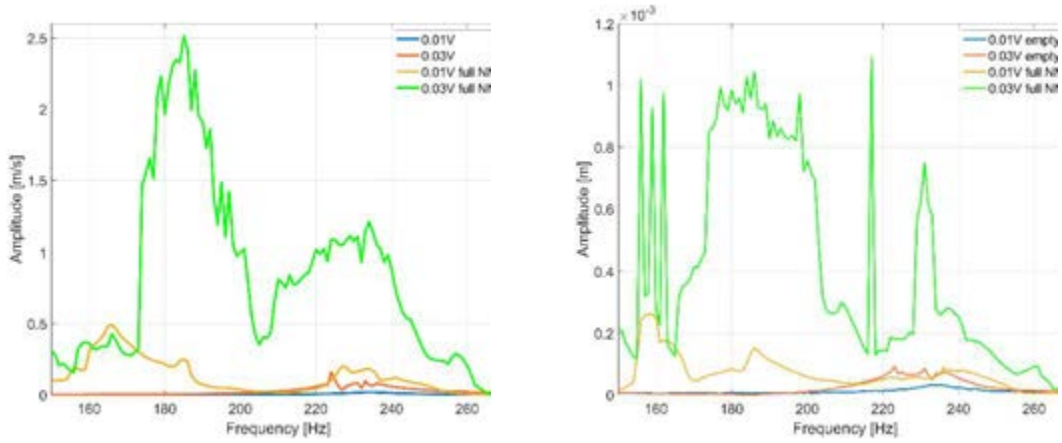

Fig. 5. Empty shell VS NN fluid-filled shell: frequency-response curve comparison at different excitation amplitudes. (a) shaker base vertical acceleration, (b) top disk vertical acceleration, (c) shell lateral velocity, and (d) shell lateral displacement.

3.2.2. Fluid-Structure Interaction in the presence of a non-Newtonian fluid: bifurcation analysis of the full filled shell

For the case of periodically forced shell full filled by the NN fluid a bifurcation analysis has been carried out, and the results are given and discussed by considering the forcing frequency as the bifurcation parameter.

By keeping constant the shaker input voltage (0.01 V – 0.08 V) and varying the forcing frequency within the range 150-270 Hz, the dynamic scenario is analysed for specific regimes where the most interesting complexities have been observed. In particular, to identify periodic patterns or chaos in the oscillations, the following signal features are shown: frequency response curves, bifurcation diagrams, time histories, spectra, phase portraits and Poincaré maps.

The frequency response curves for the downward stepped-sine tests are given in Fig. 6(a, d). For a shaker input voltage of 0.001 V (blue lines), the response is regular all over the frequency range, with peaks in proximity of the vibration modes. For a shaker input voltage of 0.02 V (orange lines), a parametric resonance arises in the range of 179-209 Hz leading to a sudden activation of the lateral vibrations. The curves envelope around the resonance peak of the axisymmetric mode (238.77 Hz) shows a softening behaviour, and strongly nonlinear vibrations with shell amplitude displacements of about ten times the shell thickness can be observed in Fig. 6(d).

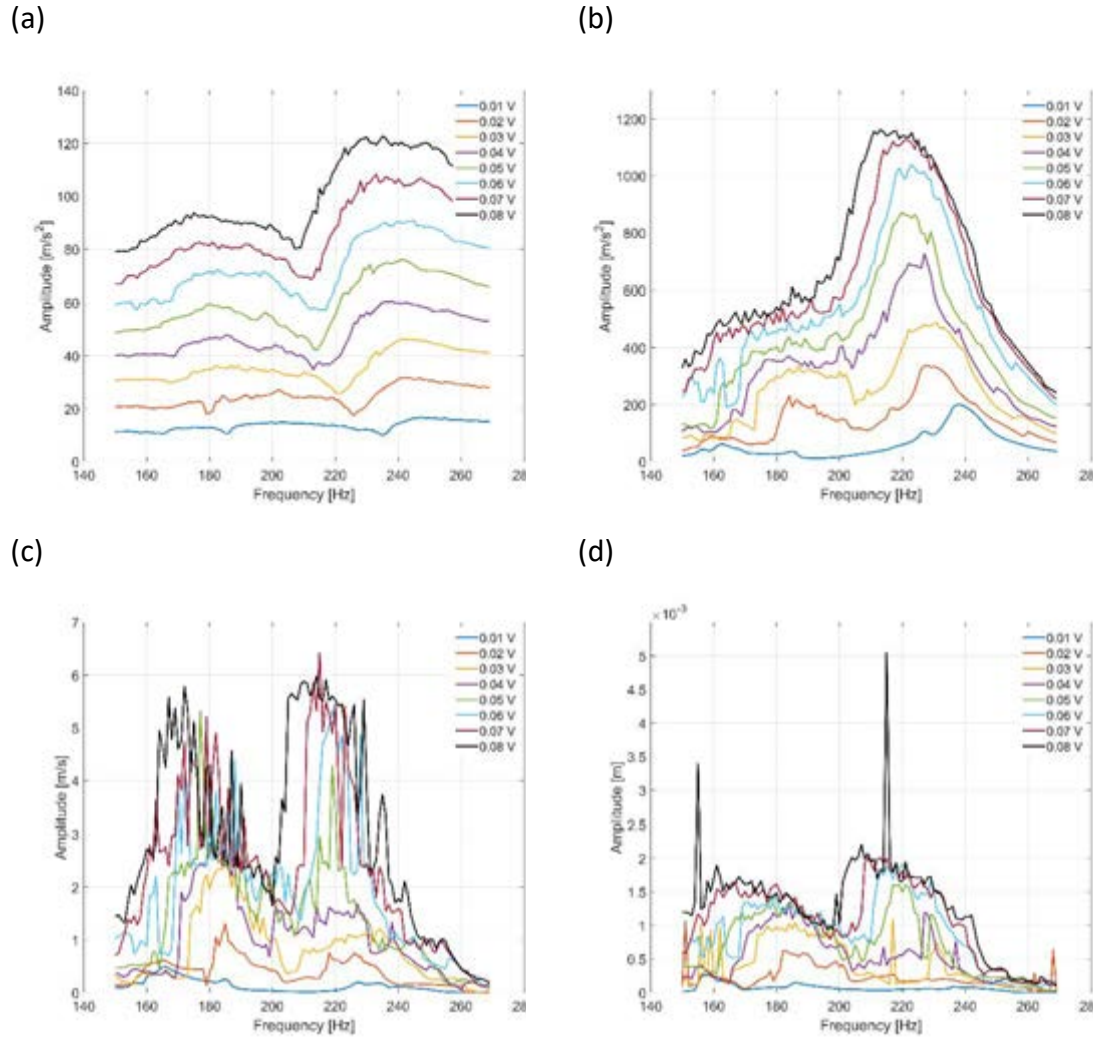

Fig. 6. Full-filled shell with oobleck. Frequency-response curves at different excitation amplitudes. (a) base acceleration, (b) top disk vertical acceleration, (c) shell lateral velocity, and (d) shell lateral displacement.

Fig. 7(a, b) show the bifurcation diagrams of the Poincaré sections computed by using the top mass acceleration in the vertical and circumferential direction, respectively, while the shell radial displacement and velocity bifurcation diagrams are given in Fig. 7(c, d), respectively. The base excitation input signal level is 0.06 V, and the frequency varies in the downward direction. The dynamic scenario is extremely rich and different sub-harmonic responses (1/2, 1/3, 1/4, 1/8), quasiperiodic and chaotic vibrations can be observed. In the velocity diagram some spurious spikes are present induced by reflection effects due to the shell surface lateral movement, see Fig. 7(d).

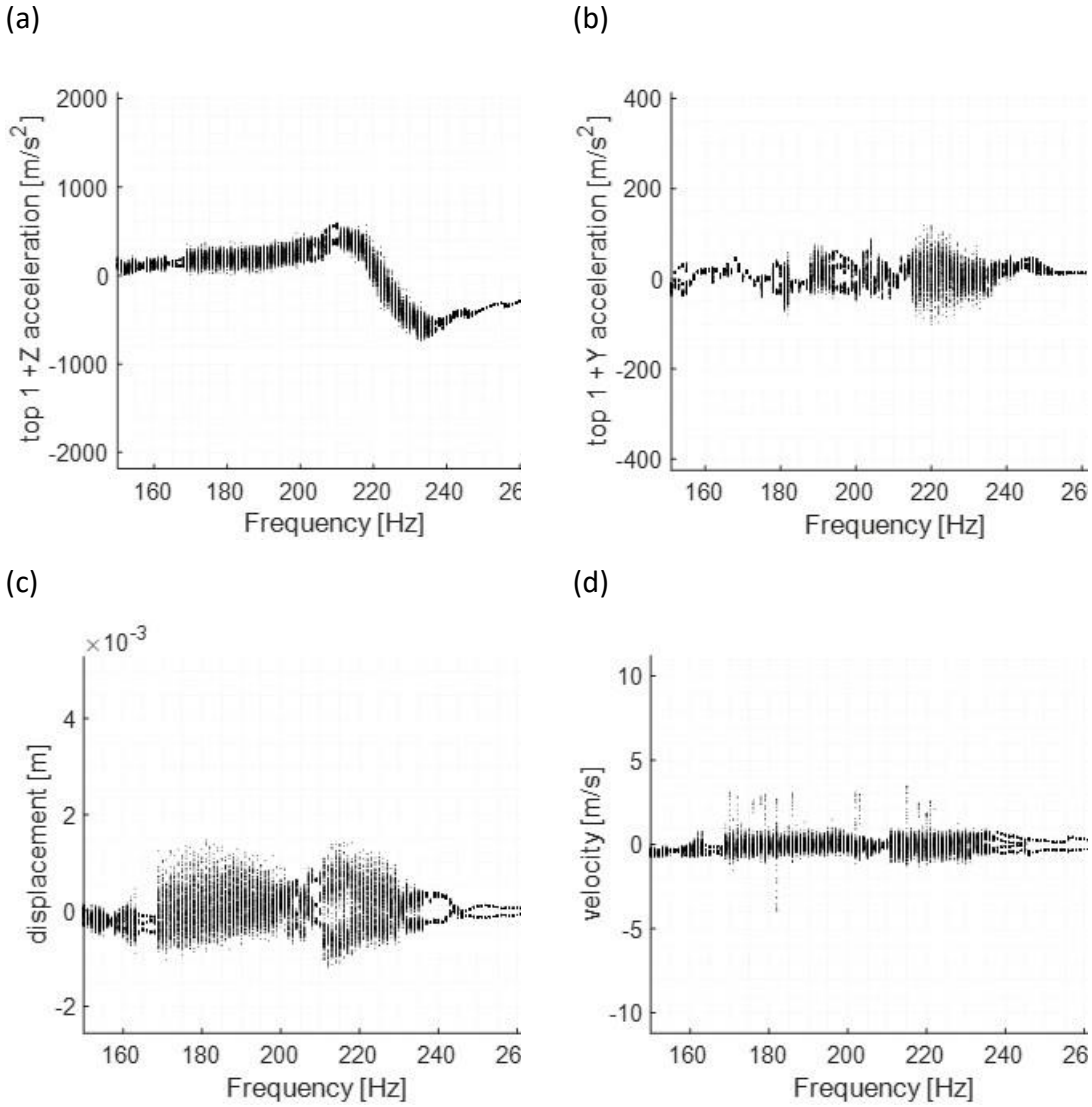

Fig. 7. Full-filled shell. Shaker input voltage 0.06 V. Downward frequency variation. Bifurcation Diagrams of the Poincaré maps. Top disk (a) vertical and (b) circumferential accelerations, shell lateral (c) displacement and (d) velocity.

Fig. 8(a, b) show the bifurcation diagrams considering a base excitation input signal of 0.06 V and an increasing forcing frequency. Between 200Hz and 215Hz, the vertical response of the system is governed by sub-harmonic oscillations. In particular, 4T-subharmonic oscillations take place at 202 Hz and 244 Hz, while the system response at 207 Hz is 2T subharmonic with amplitude modulation, see Fig. 9, where the Poincaré is given by using the top mass acceleration in the vertical and circumferential directions.

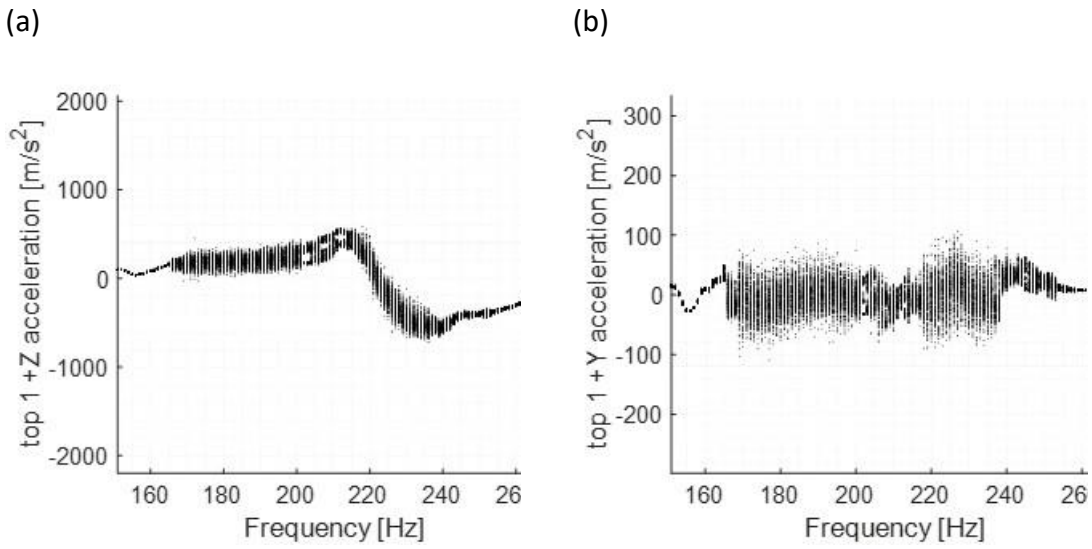

Fig. 8. Full-filled shell. Shaker input voltage 0.06 V. Upward frequency variation. Bifurcation Diagrams of the Poincaré maps. Top disk (a) vertical and (b) circumferential accelerations.

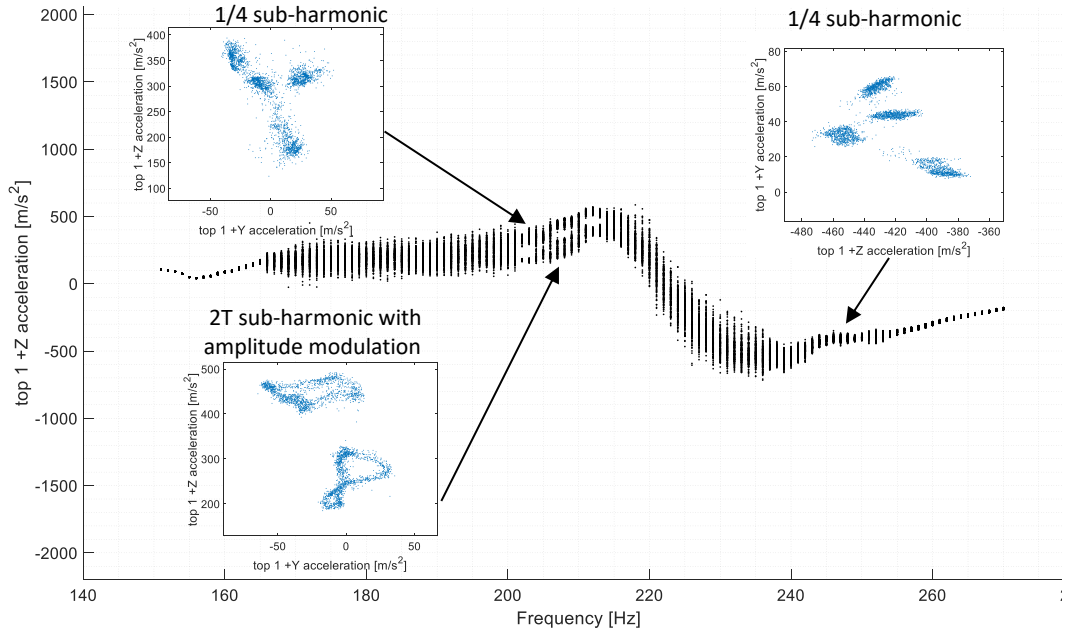

Fig. 9. Full-filled shell. Shaker input voltage 0.06 V. Upward frequency variation. Bifurcation Diagrams and Poincaré map evolution.

Fig. 10 (a, b) show the bifurcation diagrams obtained from the Poincaré sections computed by using the top mass acceleration in the vertical and circumferential directions, respectively. The base excitation input signal level is 0.07 V of a stepped sine between 150 Hz and 270 Hz with a resolution of 1 Hz in the downward direction. The response is unstable as can be seen from the top mass circumferential acceleration.

More in detail in Fig. 11, the system response at 205 Hz and 245 Hz exhibits 4T and 5T subharmonic oscillations, respectively.

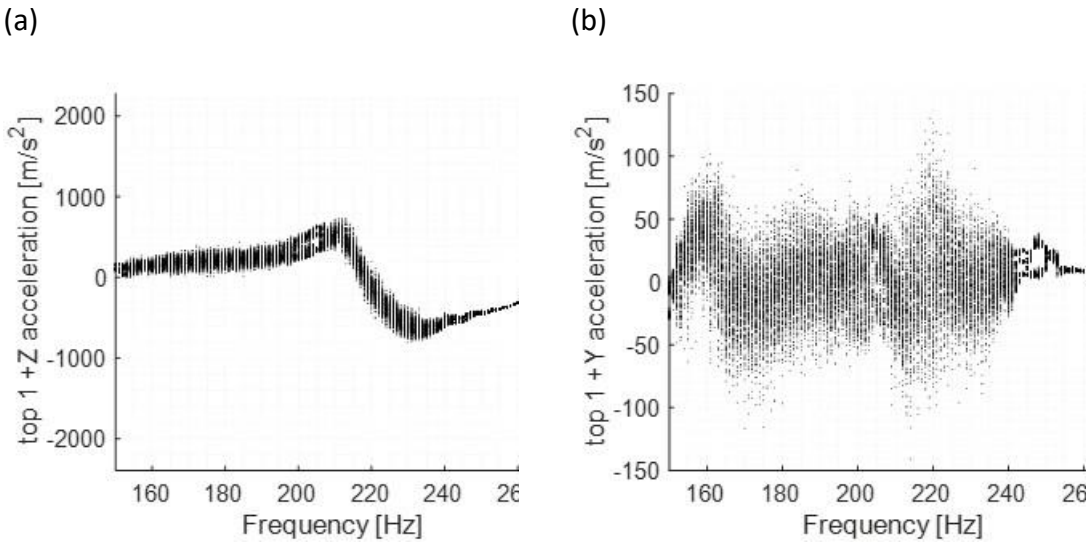

Fig. 10. Full-filled shell. Shaker input voltage 0.07 V. Downward frequency variation. Bifurcation Diagrams of the Poincaré maps. Top disk (a) vertical and (b) circumferential accelerations, shell lateral (c) displacement and (d) velocity.

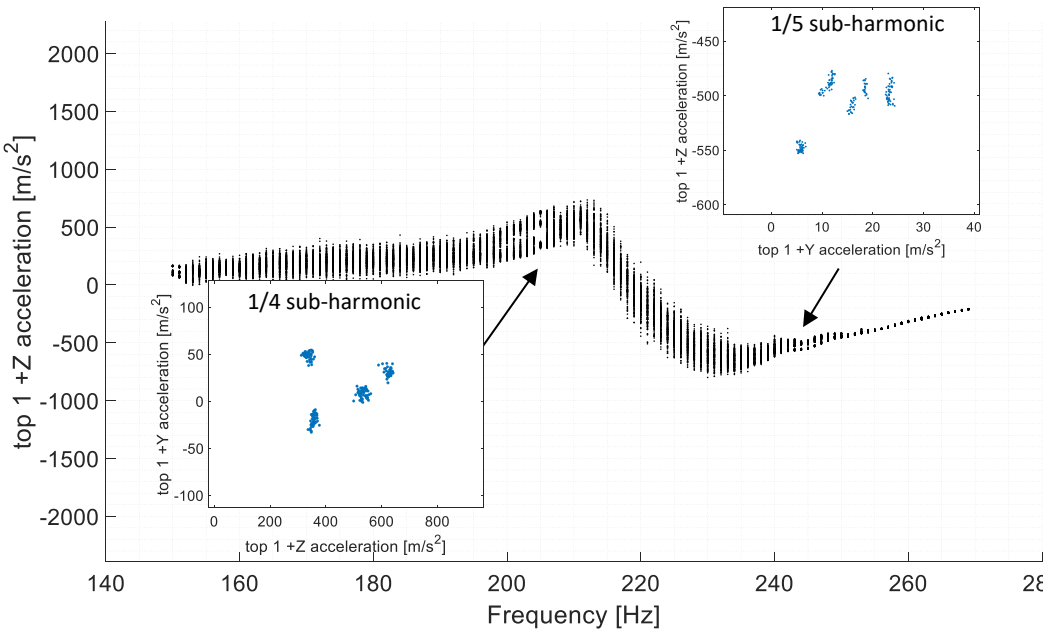

Fig. 11. Full-filled shell. Shaker input voltage 0.07 V. Downward frequency variation. Bifurcation Diagrams and Poincaré map evolution.

Fig. 12(a-d) show the bifurcation diagrams obtained from Poincaré sections computed by using the top mass acceleration in the vertical and circumferential directions, the radial displacement, and the radial velocity of the shell, respectively. The

base excitation input signal is 0.07 V (upward stepped sine test). Different sub-harmonic, quasiperiodic and chaotic responses have been observed and highlighted in Fig. 13: at 216 Hz a period doubling is present but it seems yet to move towards a chaotic behaviour; at 217 Hz and 250 Hz the motion is chaotic; a quasiperiodic response appears at 263 Hz, as shown by the Poincaré maps of the velocity and circumferential acceleration.

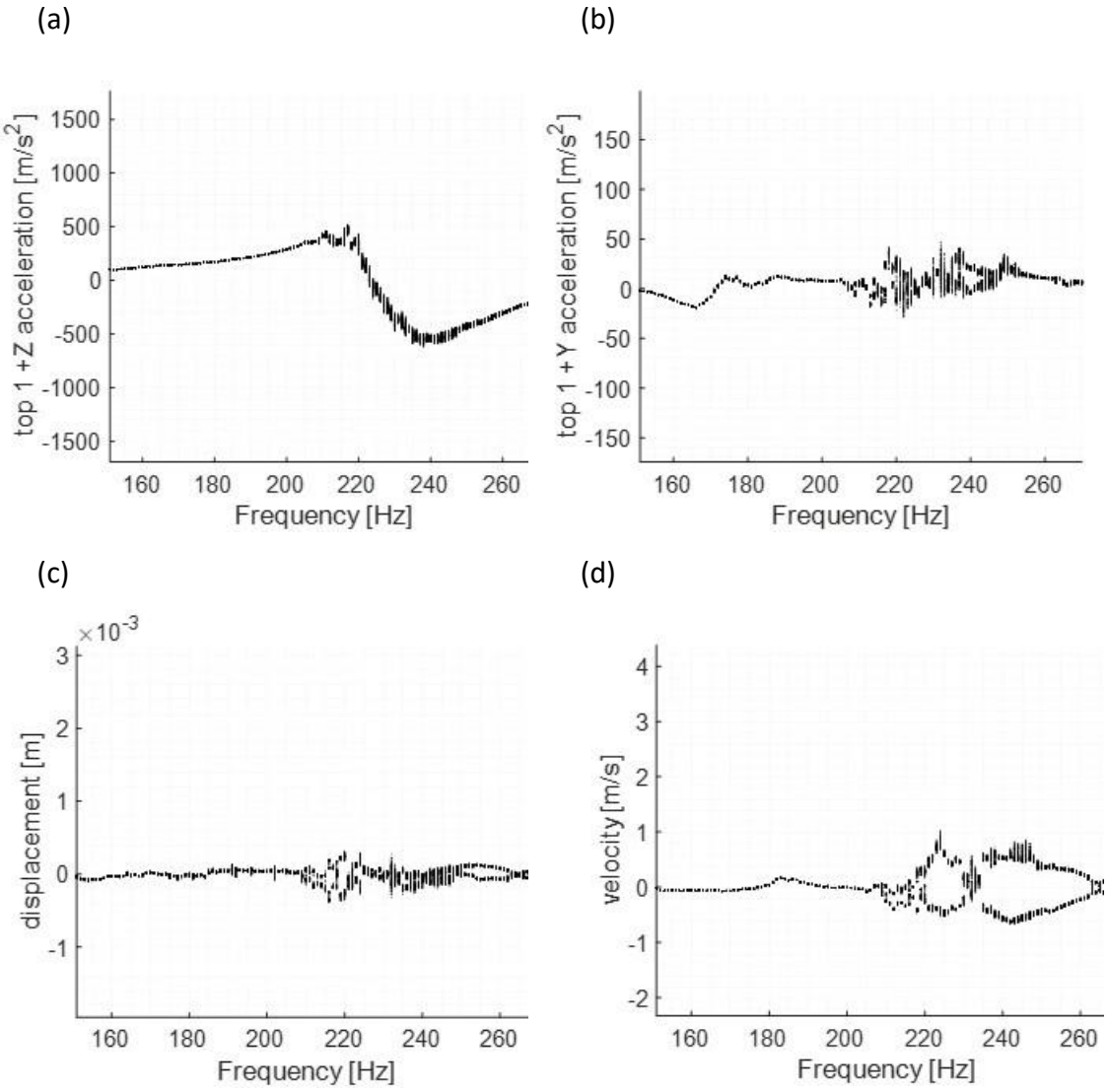

Fig. 12. Full-filled shell. Shaker input voltage 0.07 V. Upward frequency variation. Bifurcation Diagrams of the Poincaré maps. Top disk (a) vertical and (b) circumferential accelerations, shell lateral (c) displacement and (d) velocity.

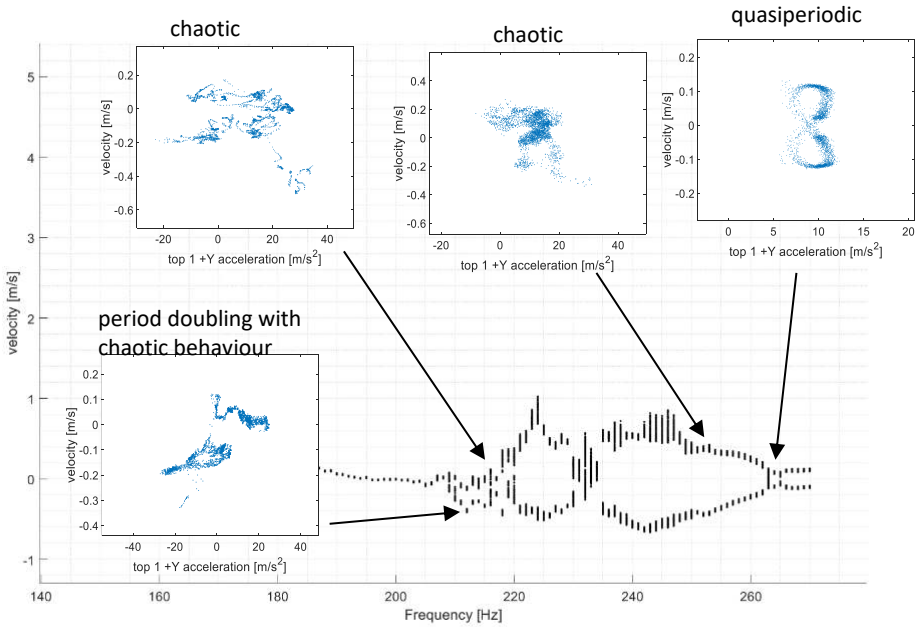

Fig. 13. Full-filled shell. Shaker input voltage 0.07 V. Upward frequency variation. Bifurcation Diagrams and Poincaré map evolution.

By increasing the input voltage up to 0.08 V, and considering an upward frequency sweep, the bifurcation diagrams are displayed in Fig. 14(a, d). At this level of excitation, all the frequency range appears unstable. In Fig. 15 is highlighted the response at 239Hz and 249 Hz. The bifurcation diagram of the response of the shell radial velocity shows 3T and 4T subharmonic responses at 239 Hz and 249 Hz, respectively.

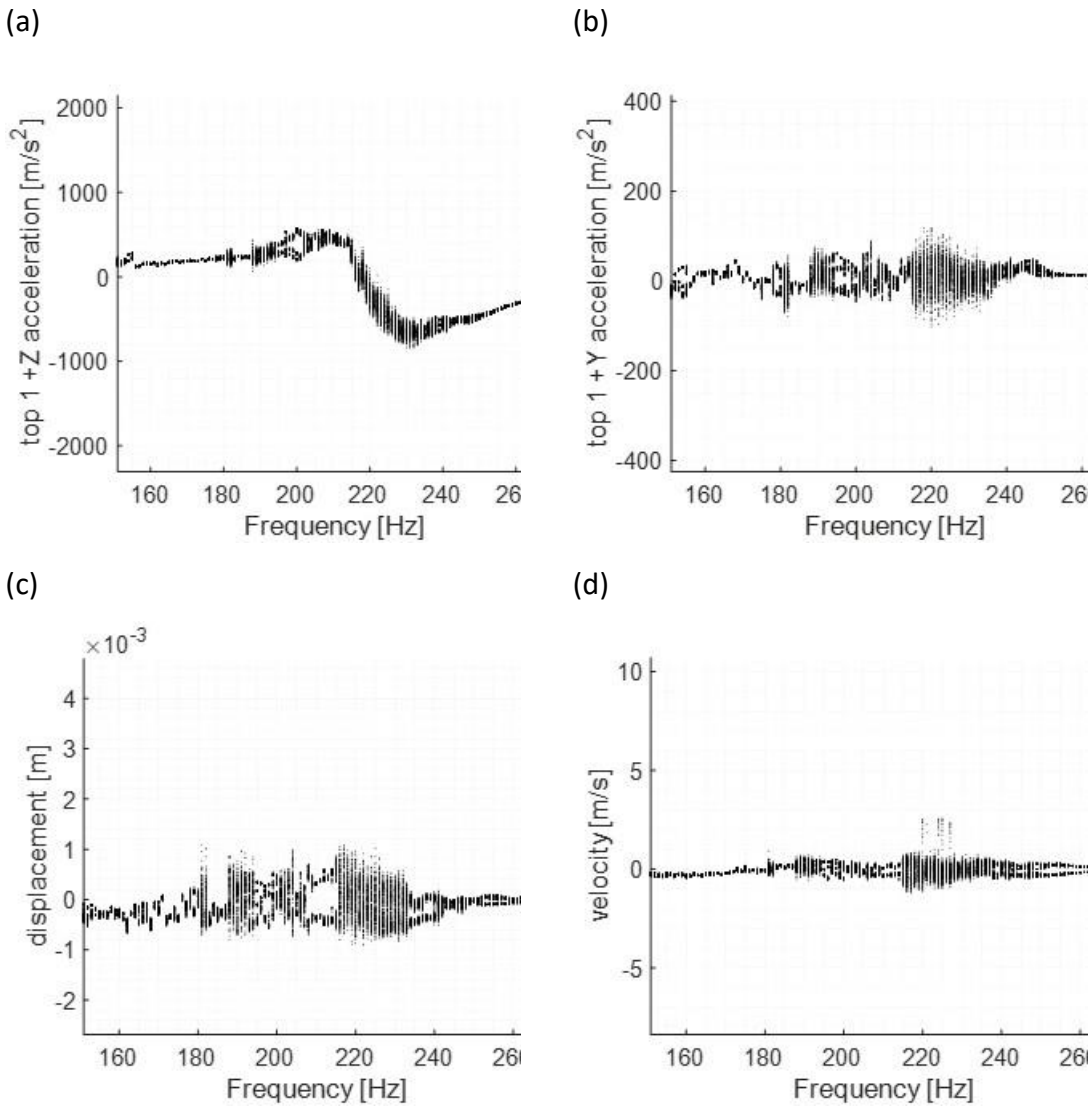

Fig. 14. Full-filled shell. Shaker input voltage 0.08 V. Upward frequency variation. Bifurcation Diagrams of the Poincaré maps. Top disk (a) vertical and (b) circumferential accelerations, shell lateral (c) displacement and (d) velocity.

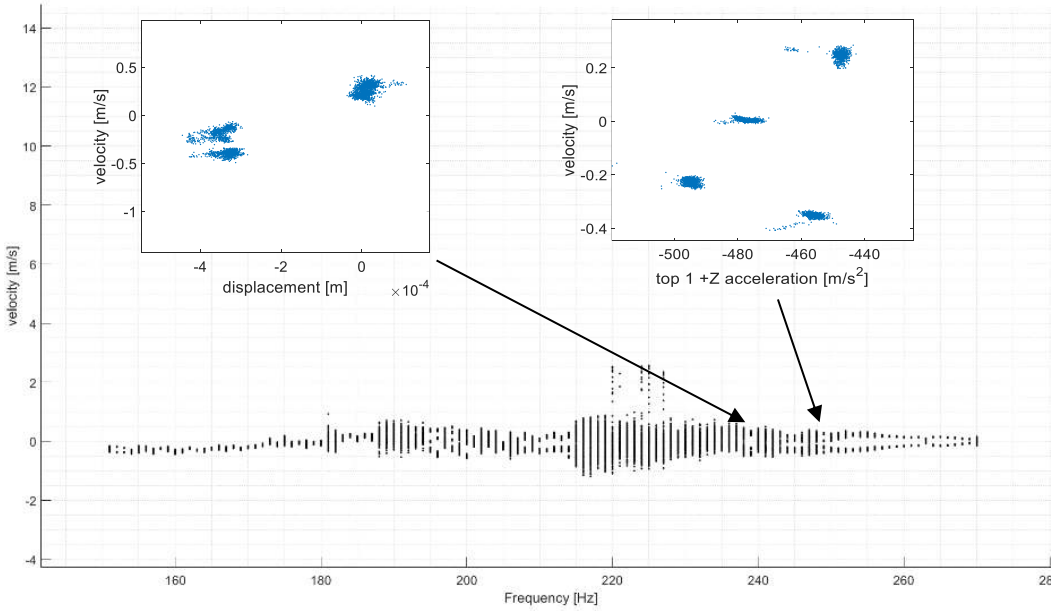

Fig. 15. Full-filled shell. Shaker input voltage 0.08 V. Upward frequency variation. Bifurcation Diagrams and Poincaré map evolution.

Considering the following settings for the drive input: voltage 0.06 V, forcing frequency equal to 242 Hz, and downward frequency sweep. The time histories of the top mass vertical acceleration and shell radial velocity in Fig. 16(a) and Fig. 16(d), respectively, show periodic oscillations. The response is 4T-subharmonic, as displayed by the spectra with peaks at 60.5Hz and its multiples, Fig. 16 (b, e), and yet confirmed by the phase plane trajectory and the 4 sets in the Poincaré section, Fig. 16(c, f), respectively.

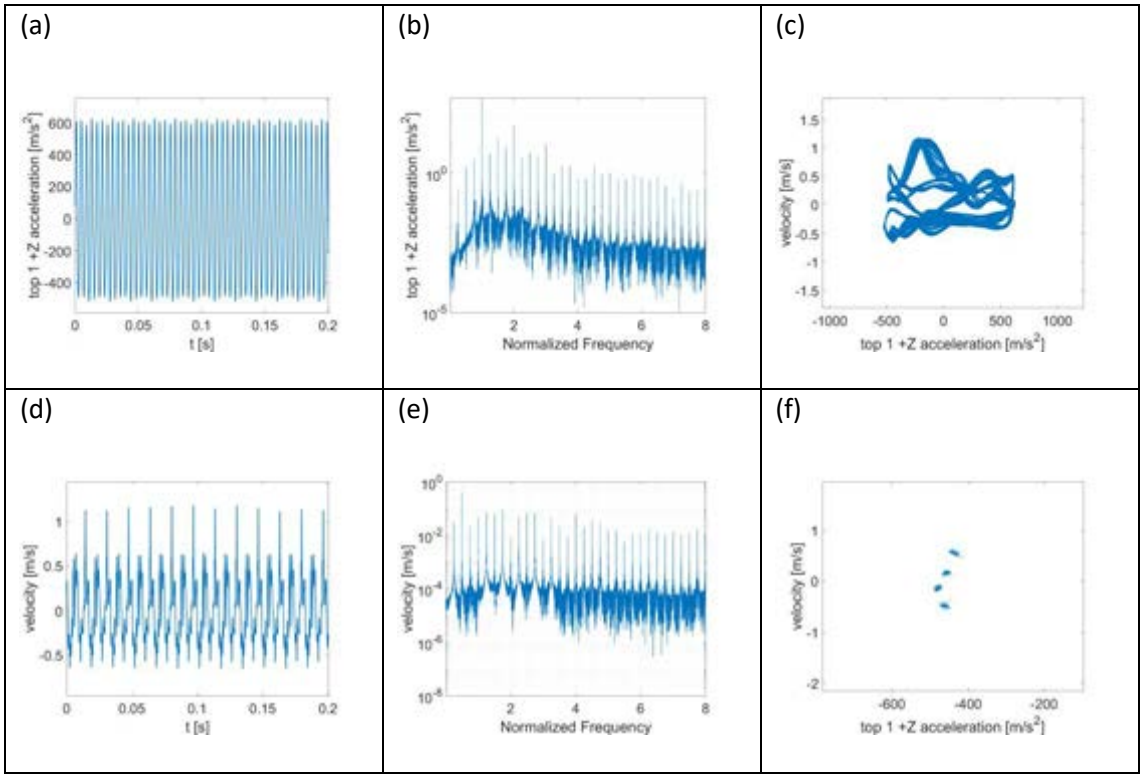

Fig. 16. Full-filled shell. Shaker input voltage 0.06 V, 242 Hz, downward. 1/4 subharmonic response. (a, d) time histories, (b, e) FFT spectra, (c) phase-plane, and (f) Poincaré map.

For a drive frequency of 169 Hz, there is clear evidence of a nonstationary and irregular response, see Fig. 17(a-f). Non-recursive patterns are shown by the time histories of the top mass vertical acceleration and shell lateral displacement, Fig. 17(a, d), respectively. The spectra show the carrier frequency at 169Hz accompanied by 1/3 and 2/3 subharmonics and superharmonics, with a high level of noise present overall in the spectra. The phase portrait, Fig. 17(c), shows an irregular orbit while the Poincaré map shows an irregular set of points, with three limited dense regions, this proves the weakly chaotic response with a 1/3 subharmonic dominant content.

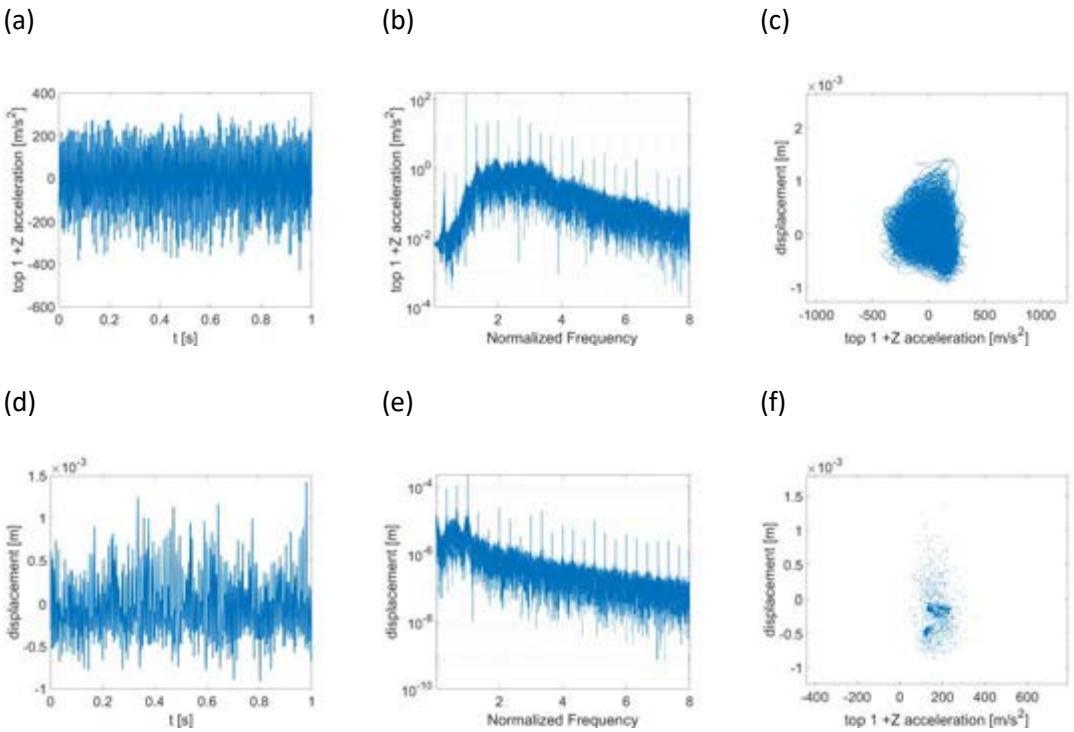

Fig. 17. Full-filled shell. Shaker input voltage 0.06 V, 169 Hz, downward. Chaotic response with 1/3-subharmonic content. (a, d) time histories, (b, e) FFT spectra, (c) phase-plane, and (f) Poincaré map.

For a drive frequency of 168 Hz, Fig. 18(a-f), the response is still subharmonic but a slight amplitude modulation is visible in the shell radial displacement time history, Fig. 18(d). In Fig. 18(b, e), the spectra confirm the 1/3 subharmonic frequency at 56 Hz, corresponding to 1/3 of the excitation frequency and sidebands of about 10 Hz. The phase portrait shows an almost closed orbit, Fig. 18(c), the Poincaré map clarifies that the 1/3 subharmonic response is also amplitude modulated, indeed, it shows three closed orbits.

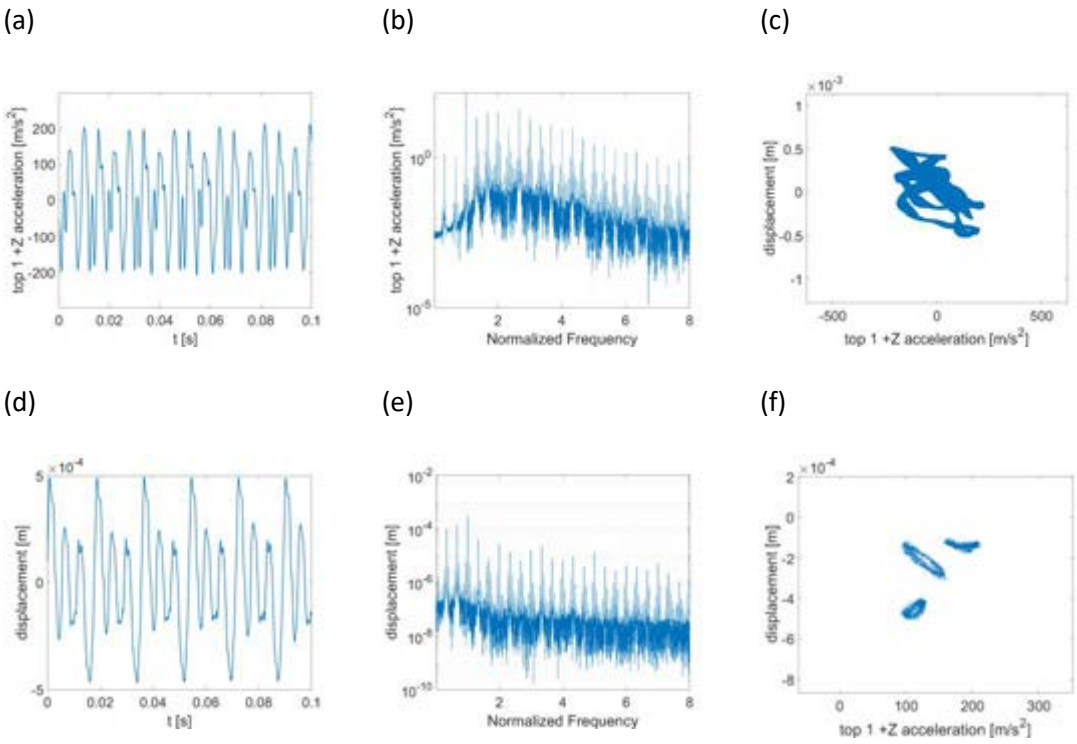

Fig. 18. Full-filled shell. Shaker input voltage 0.06 V, 168 Hz, downward. 1/3 subharmonic response with amplitude modulation. (a, d) time histories, (b, e) FFT spectra, (c) phase-plane, and (f) Poincaré map.

By reducing the drive frequency to 167 Hz, 1/3 subharmonic response occurs, see Fig. 19(a-f). The spectra show peaks at 55.67 Hz (and multiples) and the periodicity is confirmed by the closed orbit in the phase portrait as well as by the 3 sets displayed by the Poincaré section.

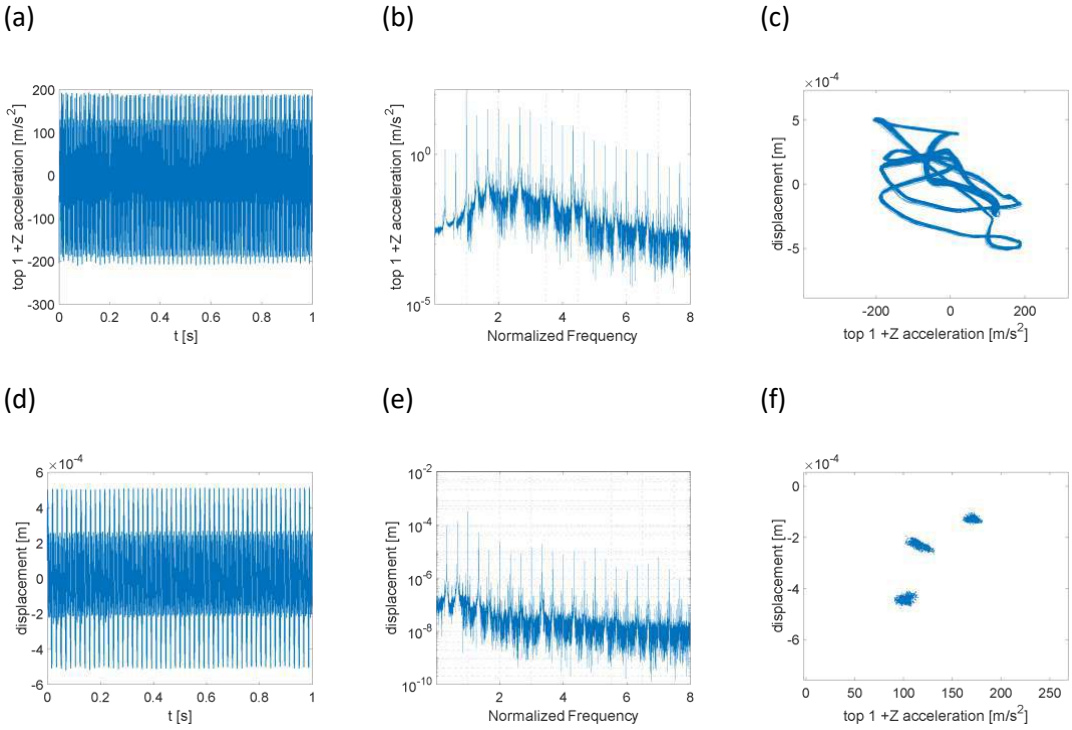

Fig. 19. Full-filled shell. Shaker input voltage 0.06 V, 167 Hz, downward. 1/3 subharmonic response. (a, d) time histories, (b, e) FFT spectra, (c) phase-plane, and (f) Poincaré map.

Fig. 20(a-f) show details of the dynamic response for an excitation frequency of 160Hz for the downward stepped sine test. Fig. 20(a, d) show the time histories of the vertical acceleration of the top disk and the lateral displacement of the shell, respectively. There is clear evidence of a quasiperiodic response with a beating period of about 0.17 s, i.e., about 7.2 Hz beating frequency. This is confirmed by the Fourier spectra, Fig. 20(b, e), where can be observed the carrier frequency at 160Hz corresponding to the excitation frequency, and the sidebands spaced of 7.2Hz correspond to the beatings in the time histories. The phase portrait Fig. 20(c) shows an orbit that fills a portion of the phase space; unfortunately, the Poincaré map is quite polluted and seems to show a closed curve, see Fig. 20(f).

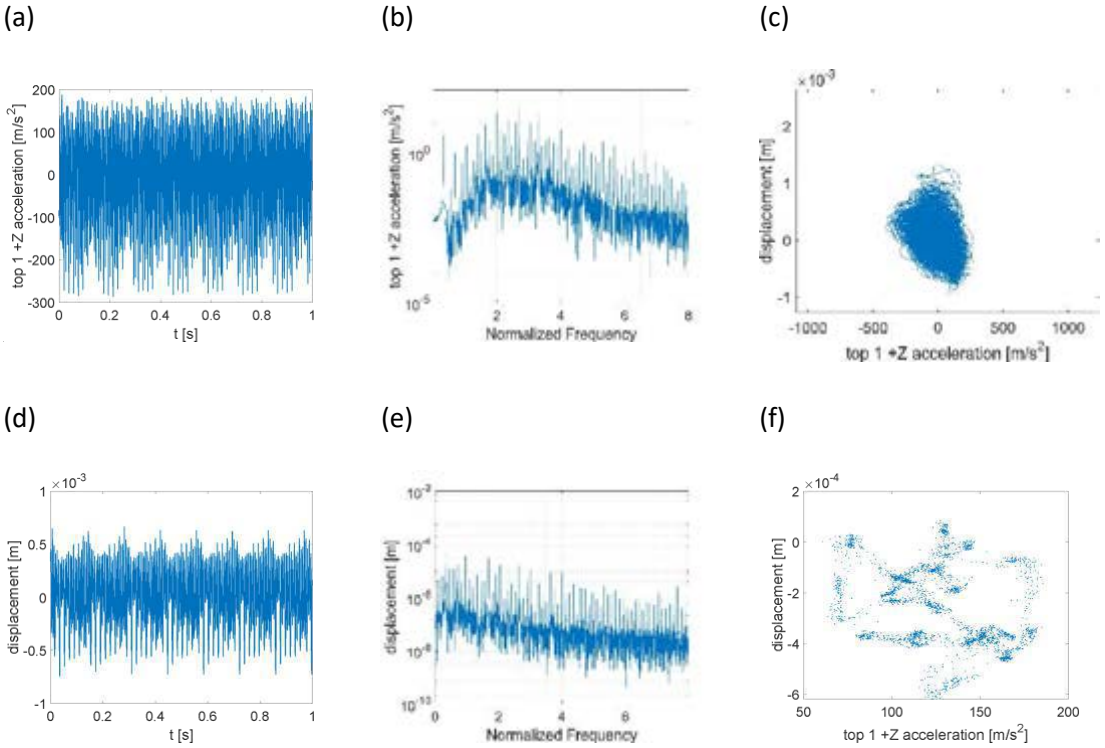

Fig. 20. Full-filled shell. Shaker input voltage 0.06 V, 160 Hz, downward. Quasiperiodic response. (a, d) time histories, (b, e) FFT spectra, (c) phase-plane, and (f) Poincaré map.

The case of 0.06V upward exhibits strong analogies with the 0.06V downward case. In Fig. 21(a-e), a sequence of Poincaré maps shows how a small frequency variation gives rise to impressive changes: at 207Hz, a 1/2 subharmonic with amplitude modulation can be observed; at 208Hz a chaotic response with 1/2 subharmonic dominant character takes place; at 209 Hz the chaotic response loses the 1/2 subharmonic component, at 210Hz the response is still chaotic with a strong quasiperiodic feature; at 211Hz the chaotic behaviour is disappearing and the response is 1/3 subharmonic.

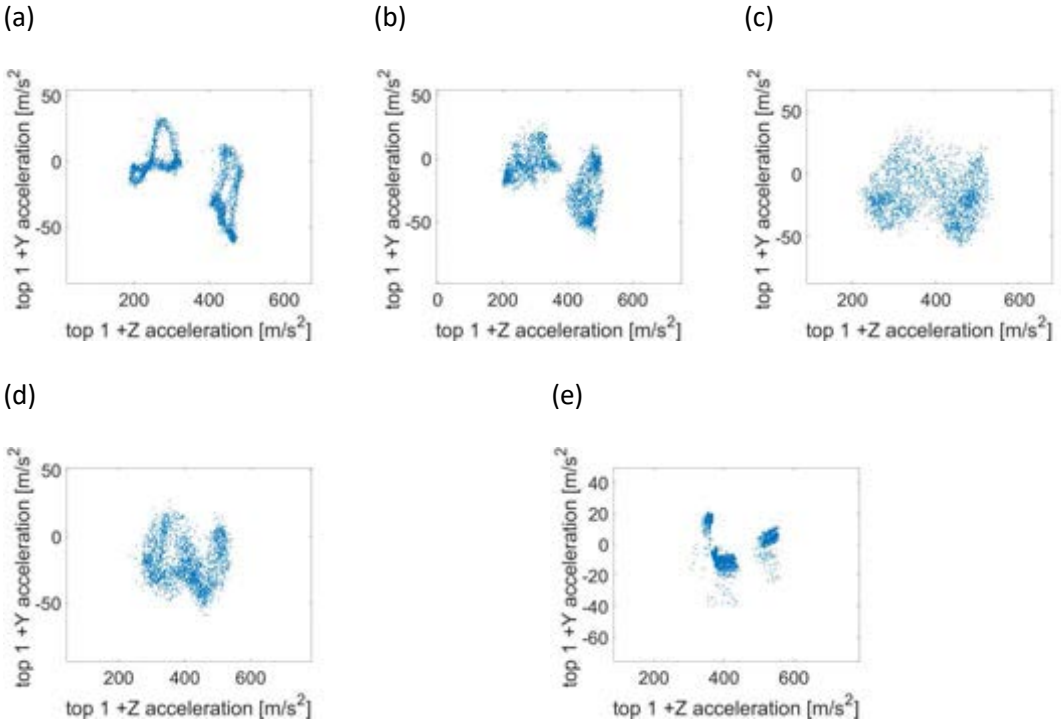

Fig. 21. Full-filled shell. Shaker input voltage 0.06 V, upward. Sequence of Poincaré maps at (a) 207 Hz, (b) 208 Hz, and (c) 209 Hz, (d) 210 Hz, and (e) 211 Hz.

Considering a shaker input voltage of 0.07 V along with an upward frequency sweep, some of the most interesting Poincaré sections are shown in Fig. 22(a-c). The representations are selected in order to show the best projection of the map in a 2D figure. In Fig. 22(a) the map, given in terms of the top disk vertical acceleration and shell lateral vibration, shows a chaotic regime modulated by a 1/2 subharmonic. Fig. 22(b) shows an irregular map (shell lateral vibration vs top disk circumferential acceleration), probably having a fractal character, representing a chaotic response. In Fig. 22(c), the quasiperiodic oscillation is modulated for the lateral velocity at 1/4 subharmonic.

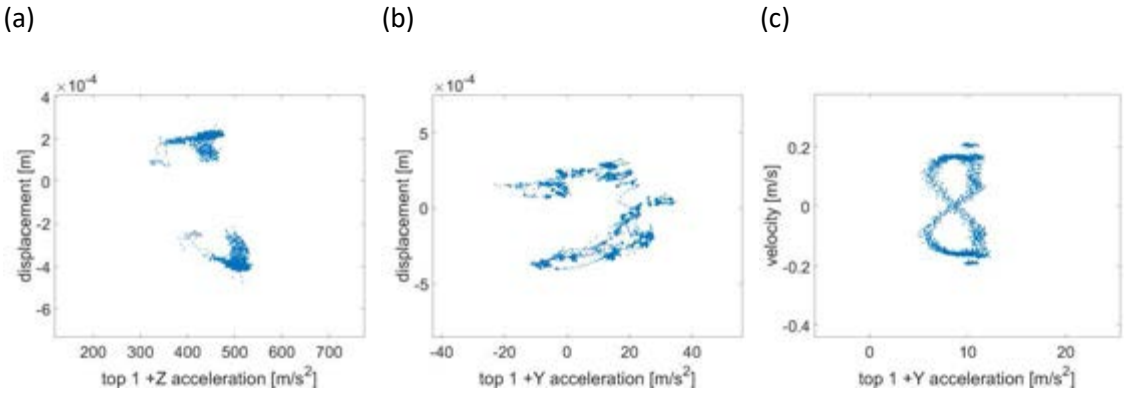

Fig. 22. Full-filled shell. Shaker input voltage 0.07 V, upward. Sequence of Poincaré maps at (a) 216 Hz, (b) 217 Hz, and (c) 262 Hz.

For an excitation level of 0.07 V, excitation frequency 199 Hz and downward frequency sweep, the results are given in Fig. 23(a-f). Fig. 23(a) and Fig. 23(d) show the time histories of the top disk vertical and circumferential accelerations, respectively, where the response is nonstationary and irregular. Fig. 23(b) and Fig. 23(e) show the spectra of the signals, the carrier frequency of 199Hz is present and the spectrum is dominated by noise. The phase portrait, Fig. 23(c), shows an irregular orbit and the Poincaré map is an irregular, without any evident shape or specific accumulation of points, see Fig. 23(f).

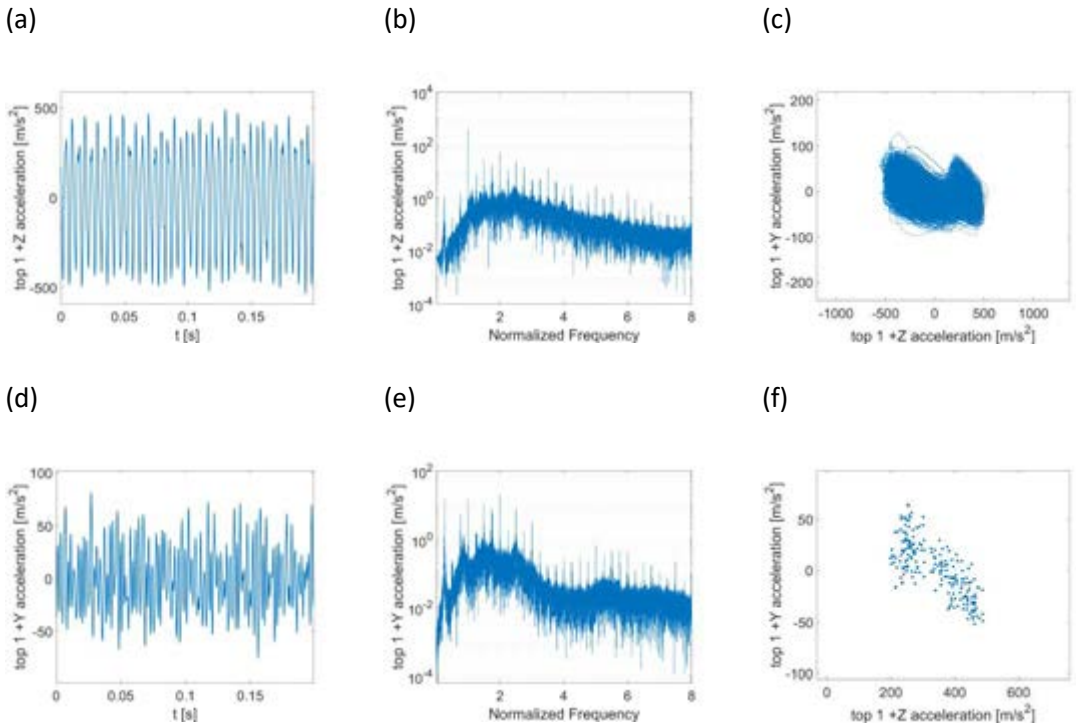

Fig. 23. Full-filled shell. Shaker input voltage 0.07 V, 199 Hz, downward. Chaotic response. (a, d) time histories, (b, e) FFT spectra, (c) phase-plane, and (f) Poincaré map.

For a drive input amplitude of 0.08 V, a forcing frequency equal to 241 Hz and a downward frequency sweep, the dynamic scenario is given in Fig. 24(a-d). From the analysis of the time histories, Fig. 24(a, d), and spectra, Fig. 24(b, e), of the top mass vertical acceleration and shell lateral vibration, the system response is 2T-subharmonic with a broadband noise distribution. This is in agreement with the irregular trajectory

within the phase plane, Fig. 24(c), and the two weakly sparse sets shown by the map, Fig. 24(f).

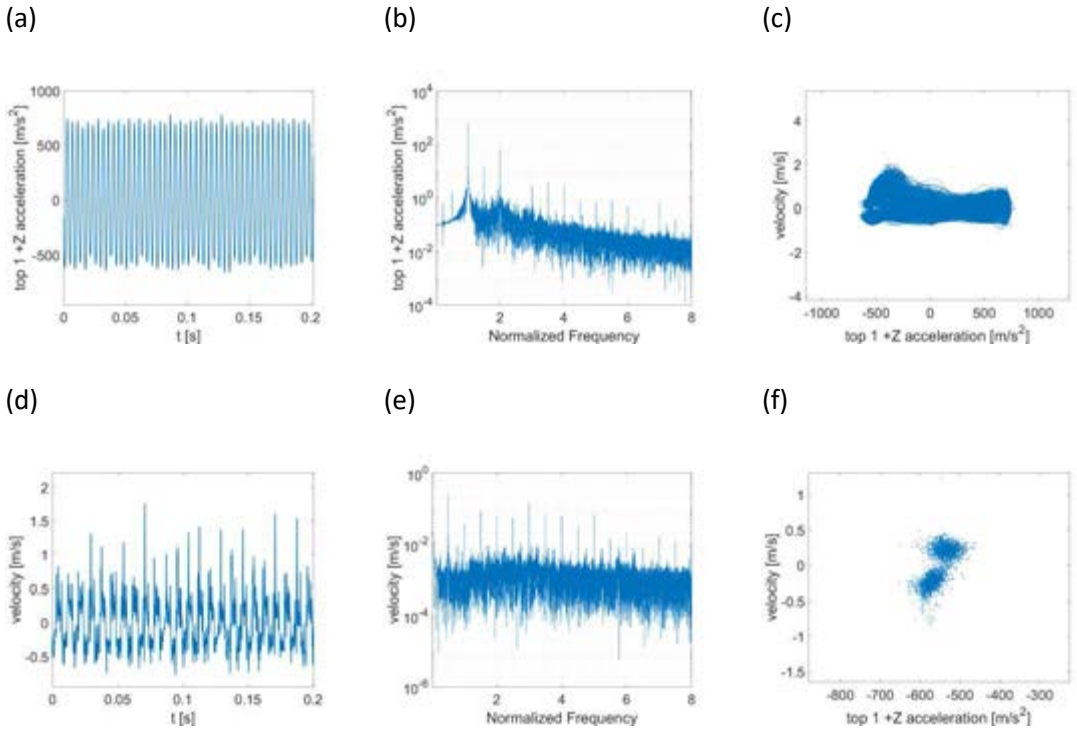

Fig. 24. Full-filled shell. Shaker input voltage 0.08 V, 241 Hz, downward. Chaotic response. (a, d) time histories, (b, e) FFT spectra, (c) phase-plane, and (f) Poincaré map.

Fig. 25(a, d) show the time histories of the top disk vertical acceleration and shell lateral vibration, respectively, for a drive input amplitude of 0.08 V, a forcing frequency of 177 Hz and an upward frequency sweep. The top disk presents a time history with irregular amplitude modulation, while the lateral vibration shows an irregular behaviour, with an evident amplitude jump at t = 0.08 s. This behaviour is probably due to the internal change of the state in the contained fluid, and it did not affect the top disk motion. Further evidence of this fluid-solid transition lies (i) in the spectra, Fig. 25(b, e), where a strong 1/2 subharmonic component is present only in the shell lateral vibration, Fig. 25(e), and (ii) in the strange attractor with a coherent fractal structure, see Fig. 25(c, f).

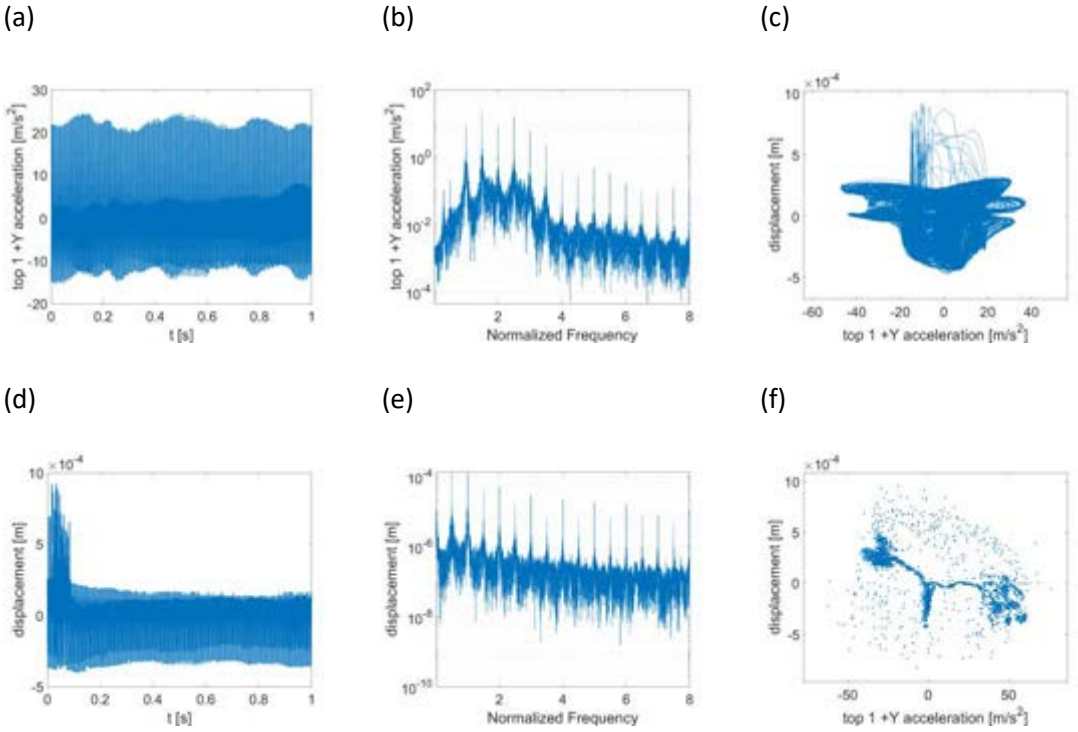

Fig. 25. Full-filled shell. Shaker input voltage 0.08V, 177 Hz, upward. Chaotic response with fluid-solid phase transition. (a, d) time histories, (b, e) FFT spectra, (c) phase-plane, and (f) Poincaré map.

4. Conclusions

In this paper, an extensive experimental campaign focused on the analysis of the dynamic interactions between an elastic structure and a non-Newtonian fluid, has been presented. A polymeric circular cylindrical shell filled with corn starch-water mixture, i.e. oobleck, under the action of a seismic resonant excitation is investigated. The low energy tests allowed identifying the basic system properties: natural frequencies, damping ratios, and mode shapes; this revealed how the fluid influences the vibrating properties of the systems and which modes are more sensitive to the added inertia due to the presence of the fluid. Stepped sine tests have been carried out at high excitation intensity and close to the resonance conditions of the shell. The investigation highlights how the presence of the non-Newtonian fluid induces parametric resonances in the system and how other nonlinear phenomena, such as the top mass acceleration saturation that is prominent in empty shells, are absent in the case of fluid-filled shells. The high amplitudes of vibration induced in the structure cause strong wave propagations in the fluid and the onset of complex dynamics when the fluid-solid transition takes place. The dynamic scenario reveals an exceptional complexity with alternate harmonic, sub-harmonic, quasiperiodic, and chaotic responses.

Acknowledgments

The present paper has been supported by the GRANT: FAR2020 Mission Oriented “Fluidi non-Newtoniani e Interazione Fluido Struttura / InterFlu”; CUP E99C20001160007.

References

[1]. C.D. Babcock, Shell stability, Journal of Applied Mechanics 50 (1983) 935–940.

[2]. C.R. Calladine, Understanding imperfection-sensitivity in the buckling of thin-walled shells, Thin-Walled Structures 23 (1995).

[3]. J.G. Teng, Buckling of thin shells: recent advances and trends, Applied Mechanics Reviews 49 (4) (1996) 263–274.

[4]. M. Amabili, M.P. Païdoussis, Review of studies on geometrically nonlinear vibrations and dynamics of circular cylindrical shells and panels, with and without fluid–structure interaction, Applied Mechanics Reviews 56 (2003) 349–381.

[5]. V.D. Kubenko, P.S. Koval'chuk, Nonlinear problems of the vibration of thin shells (review), International Applied Mechanics 34 (1998) 703–728.

[6]. Alijani, F., Amabili, M.: Non-linear vibrations of shells: a literature review from 2003 to 2013. Int. J. Non-linear Mech. 58, 233–257 (2014).

[7]. A.W. Leissa *Vibration of Shells*, NASA SP-288 Government Printing Office, Washington, DC (1993) (Now available from The Acoustical Society of America).

[8]. M. Amabili Nonlinear *Vibrations and Stability of Shells and Plates* Cambridge University Press, Cambridge (2008).

[9]. J.C. Yao, Dynamic stability of cylindrical shells under static and periodic axial and radial load, AIAA Journal 1 (6) (1963) 457–468.

[10]. A. Vijayaraghavan, R.M. Evan-Iwanowski, Parametric instability of circular cylindrical shells, Journal of Applied Mechanics 34 (1967) 985–990.

[11]. K. Nagai, N. Yamaki, Dynamic stability of circular cylindrical shells under periodic compressive forces, Journal of Sound and Vibration 59 (3) (1978) 425–441.

[12]. A.A. Bondarenko, P.I. Galaka, Parametric instability of Glass-plastic cylindrical shells, Soviet Applied Mechanics 13 (1977) 411–414.

[13]. F. Pellicano, M. Amabili, Stability and vibration of empty and fluid-filled circular cylindrical shells under static and periodic axial loads, International Journal of Solids and Structures 40 (2003) 3229–3251.

[14]. P.B. Goncalves, ZJGN Del Prado, Nonlinear oscillations and stability of parametrically excited cylindrical shells, Meccanica 37 (2002) 569–597.

[15]. A.A. Popov, Parametric resonance in cylindrical shells: a case study in the nonlinear vibration of structural shells, Engineering Structures 25 (2003) 789–799.

[16]. E. Jansen, Dynamic stability problems of anisotropic cylindrical shells via a simplified analysis, Nonlinear Dynamics 39 (2005) 349–367.

[17]. Amabili M. A comparison of shell theories for large-amplitude vibrations of circular cylindrical shells: Lagrangian approach. *J Sound Vib* (2003); 264: 1091–1125. DOI:10.1016/S0022-460X(02)01385-8.

[18]. Kurylov Y, Amabili M. Nonlinear vibrations of clamped-free circular cylindrical shells. *J Sound Vib* (2011); 330: 5363–5381. DOI:10.1016/j.jsv.2011.05.037.

[19]. G. Catellani, F. Pellicano, D. Dall'Asta, M. Amabili, Parametric instability of a circular cylindrical shell with geometric imperfections, Computers & Structures 82 (2004) 2635–2645.

[20]. F. Pellicano and K. V. Avramov, "Linear and nonlinear dynamics of a circular cylindrical shell connected to a rigid disk", *Communications in Nonlinear Science and Numerical Simulation*, 2007, 12(4), 496-518.

[21]. F. Pellicano, "Vibrations of circular cylindrical shells: theory and experiments", J. of Sound and Vibration, 2007, 303, 154–170. doi:10.1016/j.jsv.2007.01.022.

[22]. F. Pellicano Dynamic stability and sensitivity to geometric imperfections of strongly compressed circular cylindrical shells under dynamic axial loads, Communications in Nonlinear Science and Numerical Simulations, 2009, 14(8) (2009), 3449-3462, http://dx.doi.org/10.1016/j.cnsns.2009.01.018.

[23]. F. Pellicano, Dynamic instability of a circular cylindrical shell carrying a top mass under seismic excitation: experiments and theory, Int. J. of Solids and Structures, 48 (2011) 408–427.

[24]. F. Pellicano, M. Barbieri, Complex dynamics of Circular Cylindrical Shells, Int. International Journal of Non-Linear Mechanics 65 (2014) 196–212. http://dx.doi.org/10.1016/j.ijnonlinmec.2014.05.006.

[25]. M.P. Païdoussis, Fluid-Structure Interactions, Volume 1: Slender Structures and Axial Flow, Second Edition, ISBN: 9780123973122, Academic Press, 2014.

[26]. M.P. Païdoussis, Fluid-Structure Interactions, Volume 2: Slender Structures and Axial Flow, Second Edition, ISBN: 9780123973122, Academic Press, 2016.

[27]. M. Amabili and M.P. Païdoussis, Review of studies on geometrically nonlinear vibrations and dynamics of circular cylindrical shells and panels, with and without fluid-structure interaction, ASME Applied Mechanics Review 56(4), 2003.

[28]. W. Chu and D. Kana. 1967 A theory for nonlinear transverse vibrations of a partially filled elastic tank. AIAA Journal 5, 1828—1835.

[29]. J. Ramachandran, 1979, Non-linear vibrations of cylindrical shells of varying thickness in an incompressible fluid. Journal of Sound and Vibration 64, 97—106.

[30]. Boyarshina, L. G. 1984 Resonance effects in the nonlinear vibrations of cylindrical shells containing a liquid. Soviet Applied Mechanics 20, 765—770.

[31]. Boyarshina, L. G. 1988 Nonlinear wave modes of an elastic cylindrical shell partially filled with a liquid under conditions of resonance. Soviet Applied Mechanics 24, 528—534.

[32]. P.B. Gonçalves, R.C. Batista, Nonlinear vibration analysis of fluid-filled cylindrical shells. J. Sound Vib. 127, 133–143 (1988).

[33]. Sivak, V. F., and Telalov, A. I. 1991 Experimental investigation of vibrations of a cylindrical shell in contact with a liquid. Soviet Applied Mechanics 27, 484—488.

[34]. Chiba, M. 1993 Non-linear hydroelastic vibration of a cantilever cylindrical tank: I. Experiment (empty case). International Journal of Non-¸inear Mechanics 28, 591—599.

[35]. Chiba, M. 1993 Non-linear hydroelastic vibration of a cantilever cylindrical tank: II. Experiment (Liquid-filled case). International Journal of Non-¸inear Mechanics 28, 601—612.

[36]. Chiba, M. 1993 Experimental studies on a nonlinear hydroelastic vibration of a clamped cylindrical tank partially filled with liquid. ASME Journal of Pressure »essel 1echnology 115, 381—388.

[37]. Amabili M. Theory and experiments for large-amplitude vibrations of empty and fluid-filled circular cylindrical shells with imperfections. *J Sound Vib* (2003); 262: 921–975. DOI:10.1016/S0022-460X(02)01051-9.

[38]. Alijani F, Amabili M. Nonlinear vibrations and multiple resonances of fluid filled arbitrary laminated circular cylindrical shells. *Compos Struct* (2014); 108: 951–962. DOI:10.1016/j.compstruct.2013.10.029.

[39]. Amabili M, Balasubramanian P, Ferrari G. Travelling wave and non-stationary response in nonlinear vibrations of water-filled circular cylindrical shells: Experiments and simulations. *J Sound Vib* (2016); 381: 220–245. DOI:10.1016/j.jsv.2016.06.026.

[40]. Selmane, A., and Lakis, A. A. 1997 Non-linear dynamic analysis of orthotropic open cylindrical shells subjected to a flowing fluid. Journal of Sound and »ibration 202, 67—93.

[41]. M. Amabili, F. Pellicano and M.P. Païdoussis, "Nonlinear vibrations of Simply Supported, Circular Cylindrical Shells, Coupled to Quiescent Fluid". J. of Fluids and Structures, 12, 883-918, 1998.

[42]. M. Amabili, F. Pellicano and M.P. Païdoussis, Letter to the Editor, "Further Comments on Nonlinear Vibrations of Shells", J. of Fluids and Structures, 13(1), 159-160, 1999.

[43]. M. Amabili, F. Pellicano and M.P. Païdoussis, "Non-Linear Dynamics and Stability of Circular Cylindrical Shells Containing Flowing Fluid. Part I Stability". J. of Sound and Vibration, 225(4), 655-699, 1999.

[44]. M. Amabili, F. Pellicano and M.P. Païdoussis, "Non-Linear Dynamics and Stability of Circular Cylindrical Shells Containing Flowing Fluid, Part II: Large-Amplitude Vibrations without Flow". J. of Sound and Vibration, 228(5), 1103-1124, 1999.

[45]. M. Amabili, F. Pellicano and M.P. Païdoussis, "Non-Linear Dynamics and Stability of Circular Cylindrical Shells Containing Flowing Fluid. Part III: Truncation Effect without Flow and Experiments". J. of Sound and Vibration, 237 (4), 617-640, 2000.

[46]. M. Amabili, F. Pellicano and M.P. Païdoussis, "Non-Linear Dynamics and Stability of Circular Cylindrical Shells Containing Flowing Fluid. Part IV: Large Amplitude of Vibrations with Flow". J. of Sound and Vibration, 237(4), 641-666, 2000.

[47]. M. Amabili and F. Pellicano, “Nonlinear Supersonic Flutter of Circular Cylindrical Shells ”. AIAA Journal, 39 (4), 564-573, 2001.

[48]. M. Amabili, F. Pellicano and M.P. Païdoussis, "Nonlinear Stability of Circular Cylindrical Shells in Annular and Unbounded Axial Flow". ASME J. Applied Mechanics, 68, 827-834, 2001.

[49]. M. Amabili and F. Pellicano, "Multimode Approach to Nonlinear Supersonic Flutter of Imperfect Circular Cylindrical Shells", ASME J. of Applied Mechanics , 69, 117-129, 2002.

[50]. M. Amabili ,F. Pellicano and M. P. Païdoussis, "Non-linear dynamics and stability of circular cylindrical shells conveying Flowing fluid", Computers and Structures, 2002, 80, 899-906.

[51]. F. Pellicano, M. Amabili, "Stability and vibration of empty and fluid-filled circular cylindrical shells subjected to dynamic axial loads" Int. J. of Solids and Structures, 2003, 40, 3229-3251.

[52]. M. P. Païdoussis, “Some quandaries and paradoxes in fluid-structure interactions with axial flows”, IUTAM Symposium on Integrated Modeling of fully Coupled Fluid Structure Interactions, New Brunswick, NJ, USA, 2003.

[53]. B. Muha and S. Canić , Existence of a Weak Solution to a Nonlinear Fluid–Structure Interaction Problem Modeling the Flow of an Incompressible, Viscous Fluid in a Cylinder with Deformable Walls, *Arch. Rational Mech. Anal.* 207 (2013) 919–968 (DOI) 10.1007/s00205-012-0585-5.

[54]. P. Balasubramanian, G. Ferrari and M. Amabili, Nonlinear vibrations of a fluid-filled, soft circular shell: experiments and system identification, Nonlinear Dynamics, 1409–1418 (2020). https://doi.org/10.1007/s11071-020-06007-5.

[55]. A. A. Girchenko, V. A. Eremeyev, H. Altenbach, Interaction of a helical shell with a nonlinear viscous fluid, *International Journal of Engineering Science* 61 (2012) 53–58.

[56]. F. Kabinejadiana, D. N. Ghista, Compliant model of a coupled sequential coronary arterial bypass graft: Effects of vessel wall elasticity and non-Newtonian rheology on blood flow regime and hemodynamic parameters distribution. *Medical Engineering & Physics* 34 (2012) 860–872.

[57]. H. S. Wong, M. Mackley, S. Butler, J. Baumberg, D. Snoswell, C. Finlayson, and Q. Zhao, The rheology and processing of “edge sheared” colloidal polymer opals, J. Rheol. 58(2), 397-409 (2014).

[58]. B. Wu, Y. Gan, E. Carrera and W. Q. Chen, Three-dimensional vibrations of multilayered hollow spheres submerged in a complex fluid, J. Fluid Mech. (2019), 879, 682–715. doi:10.1017/jfm.2019.681.

[59]. Peeters B, Van Der Auweraer H, Guillaume P, et al. The PolyMAX frequency-domain method: A new standard for modal parameter estimation? Shock Vib 2004; 11: 395–409. DOI:10.1155/2004/523692.

[60]. Zippo A, Barbieri M, Iarriccio G, and Pellicano, F. Nonlinear vibrations of circular cylindrical shells with thermal effects: an experimental study. Nonlinear Dyn 2020; 99: 373–391. DOI:10.1007/s11071-018-04753-1.

Figure caption list

Fig. 1. (a) Test specimen partially filled with oobleck, and (b) shell-disk assembly technical drawing.Fig. 1. (a) Test specimen partially filled with oobleck, and (b) shell-disk assembly technical drawing.

Fig. 2. Test setup scheme: (1) electrodynamic shaker, (2) specimen, (3) top disk accelerometers, (4) laser telemeter, (5) base accelerometer, (6) laser vibrometer.

Fig. 3. Empty shell mode shapes: (a, b) cantilever beam-like mode, (c, d) first axisymmetric mode, (e, f) tilt mode, and (g, h) first shell-like mode.

Fig. 4. Sum of the experimental FRFs. (a) empty shell, (b) half-filled and (c) full-filled shell with NN fluid.

Fig. 5. Empty shell VS NN fluid-filled shell: frequency-response curve comparison at different excitation amplitudes. (a) shaker base vertical acceleration, (b) top disk vertical acceleration.

Fig. 6. Full-filled shell with oobleck. Frequency-response curves at different excitation amplitudes. (a) base acceleration, (b) top disk vertical acceleration, (c) shell lateral velocity, and (d) shell lateral displacement.

Fig. 7. Full-filled shell. Shaker input voltage 0.06 V. Downward frequency variation. Bifurcation Diagrams of the Poincaré maps. Top disk (a) vertical and (b) circumferential accelerations, shell lateral (c) displacement and (d) velocity.

Fig. 8. Full-filled shell. Shaker input voltage 0.06 V. Upward frequency variation. Bifurcation Diagrams of the Poincaré maps. Top disk (a) vertical and (b) circumferential accelerations.

Fig. 9. Full-filled shell. Shaker input voltage 0.06 V. Upward frequency variation. Bifurcation Diagrams and Poincaré map evolution.

Fig. 10. Full-filled shell. Shaker input voltage 0.07 V. Downward frequency variation. Bifurcation Diagrams of the Poincaré maps. Top disk (a) vertical and (b) circumferential accelerations, shell lateral (c) displacement and (d) velocity.

Fig. 11. Full-filled shell. Shaker input voltage 0.07 V. Downward frequency variation. Bifurcation Diagrams and Poincaré map evolution.

Fig. 12. Full-filled shell. Shaker input voltage 0.07 V. Upward frequency variation. Bifurcation Diagrams of the Poincaré maps. Top disk (a) vertical and (b) circumferential accelerations, shell lateral (c) displacement and (d) velocity.

Fig. 13. Full-filled shell. Shaker input voltage 0.07 V. Upward frequency variation. Bifurcation Diagrams and Poincaré map evolution.

Fig. 14. Full-filled shell. Shaker input voltage 0.08 V. Upward frequency variation. Bifurcation Diagrams of the Poincaré maps. Top disk (a) vertical and (b) circumferential accelerations, shell lateral (c) displacement and (d) velocity.

Fig. 15. Full-filled shell. Shaker input voltage 0.08 V. Upward frequency variation. Bifurcation Diagrams and Poincaré map evolution.

Fig. 16. Full-filled shell. Shaker input voltage 0.06 V, 242 Hz, downward. 1/4 subharmonic response. (a, d) time histories, (b, e) FFT spectra, (c) phase-plane, and (f) Poincaré map.

Fig. 17. Full-filled shell. Shaker input voltage 0.06 V, 169 Hz, downward. Chaotic response with 1/3-subharmonic content. (a, d) time histories, (b, e) FFT spectra, (c) phase-plane, and (f) Poincaré map.

Fig. 18. Full-filled shell. Shaker input voltage 0.06 V, 168 Hz, downward. 1/3 subharmonic response with amplitude modulation. (a, d) time histories, (b, e) FFT spectra, (c) phase-plane, and (f) Poincaré map.

Fig. 19. Full-filled shell. Shaker input voltage 0.06 V, 167 Hz, downward. 1/3 subharmonic response. (a, d) time histories, (b, e) FFT spectra, (c) phase-plane, and (f) Poincaré map.

Fig. 20. Full-filled shell. Shaker input voltage 0.06 V, 160 Hz, downward. Quasiperiodic response. (a, d) time histories, (b, e) FFT spectra, (c) phase-plane, and (f) Poincaré map.

Fig. 21. Full-filled shell. Shaker input voltage 0.06 V, upward. Sequence of Poincaré maps at (a) 207 Hz, (b) 208 Hz, and (c) 209 Hz, (d) 210 Hz, and (e) 211 Hz.

Fig. 22. Full-filled shell. Shaker input voltage 0.07 V, upward. Sequence of Poincaré maps at (a) 216 Hz, (b) 217 Hz, and (c) 262 Hz.

Fig. 23. Full-filled shell. Shaker input voltage 0.07 V, 199 Hz, downward. Chaotic response. (a, d) time histories, (b, e) FFT spectra, (c) phase-plane, and (f) Poincaré map.

Fig. 24. Full-filled shell. Shaker input voltage 0.08 V, 241 Hz, downward. Chaotic response. (a, d) time histories, (b, e) FFT spectra, (c) phase-plane, and (f) Poincaré map.

Fig. 25. Full-filled shell. Shaker input voltage 0.08V, 177 Hz, upward. Chaotic response with fluid-solid phase transition. (a, d) time histories, (b, e) FFT spectra, (c) phase-plane, and (f) Poincaré map.

Table caption list

Table 1. Specimen geometric dimensions and material properties.

Table 2. Numerical (FEM) and experimental mode shapes, natural frequencies (f), and linear damping ratios (ζ).